Nuno Gonçalo Rosa Roberto

Bachelor in Micro and Nanotechnologies Engineering

Influence of collagen fibril alignment in collagen scaffolds mineralization

Master of Science in

Micro and Nanotechnologies Engineering

Adviser: Dr. Miguel Dias Castilho, Associate Professor,
Department of Orthopaedics, University Medical Center Utrecht

Co-Adviser: Dr. João Paulo Borges, Associate Professor with Habilitation,
Faculty of Sciences and Technology, NOVA University of Lisbon

Examination committee:

Chairperson: Dr. Hugo Manuel Águas
Repporteurs: Dr. Jorge de Carvalho e Silva
Members: Dr. Miguel Dias Castilho

February 2021

FACULDADE DE CIÊNCIAS E TECNOLOGIA
UNIVERSIDADE NOVA DE LISBOA

Influence of collagen fibril alignment in collagen scaffolds mineralization

“Life is like a box of chocolates.”

-Forrest Gump

Acknowledgments

After 5 years of hard work, accomplishments, and losses, I am proud to say I have finished my masters in Micro and Nanotechnology Engineering. This would not be possible without the presence of very important people around me, who supported me every step of the way and gave me all the conditions I needed.

Firstly, I would like to thank Professor Dr. Miguel Castilho for all the help given, the hours spent in the lab trying to work things out, the lunches that made me feel a bit closer to home, the professionalism, and of course, for the unique opportunity to work in one of the world's best regenerative medicine institutions. All of these things made the experience one of the best experiences I ever had. I also would like to thank for changing my mind about the research world, and I hope we can be working together in the near future.

To Nasim, thanks for all the conversations, the sympathy, the inputs, and the constant availability to help me in my internship. You made everything way easier, and I wish you the best in the future, even if your future is in Spain. I also hope we can meet again someday (you must visit Portugal).

To Andrei, my Byelorussian friend and labmate. Thank you for all the moments spent in the lab, all the fixups in lab equipment, all the conversations about random stuff, and of course, Spaciba for the Russian classes. I wish you the best, and I hope to see you again sometime.

To my co-advisor, Professor Dr. João Paulo Borges, I would like to thank you for accepting to advise me in this stage of my academic path. Thank you for all the work done in our university, especially in the biomaterials field. If it were not for you, I would never have any interest in this rea, and I would never have realized that I want to do this in my future.

I also would like to thank my friends (integrating members of the NanoDilemas group) for helping me go through the last five years. I am sure that it would not have been possible to get where I am today without them, and I am positive that this is a lifetime friendship. Also, to aunt Shanon and Tixa, a huge thank you for all the time spent and the never-ending friendship.

To my Caldas friends, David, CC, Miguel, Tiz, Cacota, PP, Pinho, Zé, Mara, and Ricardo, a huge thank you for all the fun times, the coffee (beer) meetings, and all the nights that always end up in mac. Above all, thank you for making me a much happier person.

To my girlfriend, Vera, I want to thank you for being there every second of the way. You were, without a doubt, a tremendous support in the most challenging times and were also the first one there to celebrate with me when things turned out to be great. Thank you for everything and for being part of my life.

Finally, and the most important thank you. I want to thank my parents, my aunt, my sister, and my grandmother. Without you guys, nothing would be possible. Thank you for giving me the opportunity to continue my studies and all the conditions I needed to succeed, even when I decided to go abroad. Never felt I was missing something, and all thanks to you. THANK YOU

Resumo

A matrix extra celular (ECM) do osso confere-lhe as suas únicas propriedades mecânicas e, portanto, torna-se importante mimetizar a composição e microestrutura nativa da ECM em engenharia de tecidos ósseos. O colagénio tipo-I é o principal componente da ECM e funciona como suporte para adesão celular e deposição de minerais, podendo a mineralização ocorrer nos espaços Intra e interfibrilares do colagénio. Existem algumas teorias que tentam explicar os mecanismos de formação de minerais no tecido ósseo. Contudo, nenhuma foi comprovada, fazendo com que, o mecanismo pelo qual a mineralização facilitada por colagénio ocorre, seja ainda desconhecido. Desta forma, estudar este mecanismo e desenvolver técnicas, em engenharia de tecidos, para que seja possível mimetizar a ECM do osso, torna-se essencial.

Neste projeto, teorizámos que o alinhamento das fibrilas de colagénio em *scaffolds* iriam promover a sua mineralização. Deste modo, hidrogéis de colagénio fibrilar foram impressos recorrendo à técnica de impressão em suspensão, na qual foi utilizado um banho de suspensão à base de gelatina. Inicialmente, a otimização do processo de impressão foi efetuada. De seguida, as fibras mais estreitas (123 ± 25 µm) e largas (215 ± 66 µm) foram escolhidas para realizar a impressão das estruturas desejadas. Foi provado que o diâmetro das fibras influencia o alinhamento das fibrilas de colagénio nas estruturas e, consequentemente, a sua mineralização. As fibras de menor dimensão apresentaram sinais de mineralização após um dia de submersão na solução de mineralização, enquanto que, as fibras mais largas exibiram sinais de deposição de minerais apenas após três dias. Adicionalmente, a técnica de *suspended electrowriting* foi introduzida nesta dissertação, obtendo-se um diâmetro de jato de 40 µm dentro de um banho de óleo de ricínio, provando que esta é uma técnica promissora de fabrico aditivo, que nos permite atingir melhores resoluções na impressão 3D de hidrogéis.

Palavras-chave: hidrogéis, scaffolds, colagénio, Impressão em suspensão, suspended electrowriting, regeneração óssea, mineralização

Abstract

Bone extracellular matrix (ECM) gives bone its unique mechanical properties, thus being important in bone tissue engineering to mimic its native composition and microstructure. The main component in bone ECM is Type-I collagen, which works as a scaffold for bone cell attachment and mineral deposition. There are two locations where mineralization takes place: the intrafibrillar and interfibrillar spaces of collagen fibrils. Several theories try to explain mineral formation in bone tissue. However, none of them was proven right, and so, the mechanism for mineralization facilitated by the collagen lattice is still unknown. This way, it is essential to study such a mechanism and develop bone tissue engineering approaches to mimic bone ECM.

In this work, we hypothesized that collagen fibrils alignment would promote scaffolds mineralization. To prove it, we 3D printed fibrillar collagen hydrogels scaffolds using the suspension 3D printing technique, in which a gelatin slurry was used as a suspension bath. First, an optimization of the printing process was performed. Then scaffolds were printed, choosing the finest (123 ± 25 μm) and largest fiber diameter (215 ± 66 μm) obtained. Fiber diameter size was proven to affect the collagen fiber alignment inside the scaffolds and, consequently, affect mineral precipitation. The smallest fiber diameter scaffold showed signs of mineralization after one day inside a mineralization solution. In contrast, the largest fiber scaffold only presented mineralization signs after three days of submersion. Moreover, suspended electrowriting was introduced in this dissertation, obtaining a 40 μm jet diameter inside a castor oil bath, proving to be a promising additive manufacturing technology to achieve higher resolution constructs when 3D printing hydrogels.

Keywords: hydrogels, scaffolds, collagen, suspension printing, suspended electrowriting, bone regeneration, mineralization

Contents

List of Figures

List of Tables

Symbols

Ø	Diameter
ε	Dielectric Constant
η	Viscosity

Acronyms

ECM	Extracellular Matrix
HA	Hydroxyapatite
CaP	Calcium Phosphate
NCP	Non-collagenous proteins
BTE	Bone Tissue Engineering
3D	Three-Dimensional
AM	Additive Manufacturing
EHD	Electrohydrodynamic printing
PBS	Phosphate Buffered Saline
FOV	Field of View
ARS	Alizarin Red Staining
µCT	Micro Computed Tomography
FR	Flow Rate
BR	Best Resolution
WR	Worts Resolution
SEW	Suspended Electrowriting
SPR	Spreading Ratio

1. Introduction

1.1. Bone

Bone is a complex and hierarchically organized connective tissue whose functions are: generate blood cells, store minerals, enable locomotion, and protect the body's vital organs [1]. It presents five different structural organization levels (**Figure 1)** that work together to perform several mechanical, biological, and chemical functions [2]. These levels are defined as: the macrostructure, consisting of cancellous (50–90 vol % porosity) and cortical bone (< 10 vol % porosity); the mesostructure that consists of osteons; the microstructure that includes the lamellae and the Haversian canal; the sub-microstructure containing fibrillar collagen and embedded mineral; and the nanostructure consisting of the molecular structure of constituent elements (mineral, collagen, and non-collagenous organic proteins) [3], [4]. The sub-micro and nanostructure elements are essential since they form the bone extracellular matrix (ECM), which plays a vital role in bone tissue mechanical performance.

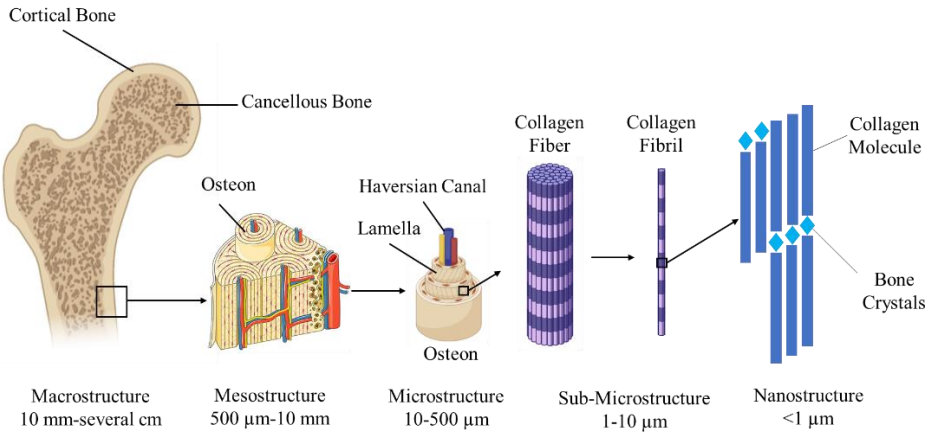

***Figure 1**-Five levels of hierarchical structural organization of bone. Adapted from* [4].

1.2. Bone Extracellular Matrix and its Mineralization

The bone extracellular matrix is a 3D structure secreted by cells into the extracellular space. Its composition and topology consist of organic components (22 wt %), inorganic crystalline mineral components (69 wt %), and water (9 wt %) [3]. The inorganic elements are represented by hydroxyapatite (HA) and calcium phosphates (CaP), which guarantee strength and toughness. On the other hand, the organic elements consist of collagenous (collagen type-I, III, and V) and non-collagenous proteins that ensure flexibility and mechanical support, acting as a scaffold for bone cells [3], [5].

Bone cells play a vital role in bone tissue regeneration. They are responsible for the constant process (bone homeostasis) that involves the resorption of old bone, mediated by osteoclasts, and deposition of new one, mediated by osteoblasts [1], [3]. New bone deposition and mineralization occur in the continuation of the existing mineralized matrix on which osteoblasts deposit unmineralized collagen (osteoid). The unmineralized collagen matrix acts as a scaffold for bone mineral deposition, having two locations where this phenomenon happens (see **Figure 2**): the intrafibrillar gap spaces (where two serially arranged collagen triple helices molecules meet) and interfibrillar spaces between the collagen fibrils [6]. However, it is mostly accepted that intrafibrillar mineralization is predominant [7].

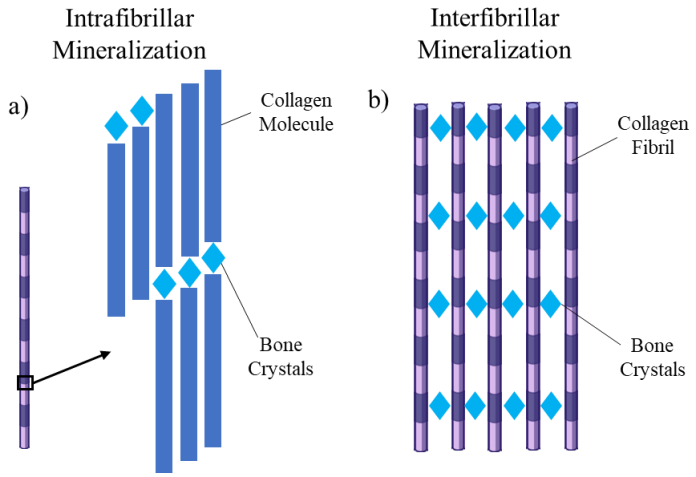

Figure 2*- a) Intrafibrillar mineralization occurs in the gaps between two successively collagen molecules. b) Interfibrillar mineralization occurs in the gaps between parallel collagen fibrils.*

It is mandatory to understand the process of mineral deposition on collagen to develop treatments for mineralization-related diseases and biomaterials for bone tissue engineering. Mineralized collagen structure is already understood. However, the mechanism behind how minerals precipitate with the spatial and hierarchical order in native tissues is still unknown [7].

There are a few theories that try to explain the mechanism where mineral deposition is facilitated. One theory defends that the amino acid chains exposed at the intrafibrillar gap space and at the interfibrillar space may regulate this process since minerals nucleate in the specific site where groups of positively and negatively charged amino acids are [7]. Another theory is that the gap regions of adjacent fibrils create channels that provide space and allow the mineral to form [8]. However, *in vitro* mineral nucleation in the collagen was observed both in the gap and overlap regions, suggesting that space's availability does not limit crystal growth [7]. In contrast, an additional theory supports that the dense packaging of collagen molecules and their hierarchical organization is the key to hydroxyapatite nucleation [6].

Non-collagenous proteins (NCPs) can also be related to the bone mineralization mechanism. Here, researchers have been studying three major approaches: systems where synthetic polymers capable of mimicking the activity of the NCPs are used (e.g., Polyaspartic acid promotes intrafibrillar mineralization [9]); models where recombinant proteins are used directly to probe the function of specific NCPs; and experiments using demineralized tissue containing matrix-bound NCPs [7]. These studies suggest that soluble macromolecules are necessary to mimic the native collagen-mineral relation. Nevertheless, none of the theories above have been confirmed. So the collagen lattice's exact mechanism facilitating mineral deposition is still unknown [6].

Despite bone ECM mineralization and regeneration mechanisms, bone intrinsic capacity for self-repair only covers minor bone defects restoration. Bone regeneration may be required in larger quantities, especially in clinical cases, or when bone repair mechanisms suffer dysregulation [10], leading to disorders that are the most frequent cause of severe long-term pain and physical incapacity, affecting millions worldwide [11]. Thus, it is vital to find a solution for bone regeneration of large defects.

1.3. Bone Tissue Engineering

Bone tissue engineering (BTE) is a multidisciplinary field where engineering and life sciences fundamentals merge. It aims to get through the downsides of conventional therapies in bone transplantation, combining living cells with a natural/artificial scaffold to develop a functional three-dimensional structure, structurally and mechanically equivalent to the tissue that is being replaced [12]. This way, scaffolds play a significant role in BTE since they are 3D porous structures that can provide mechanical support, modulate cell behavior, and extracellular matrix deposition [13].

Bone scaffolds should have: biocompatibility, so the scaffold is not rejected by the organism, and the absence of cytotoxicity is assured; osteoconductive and osteoinductive properties; mechanical properties similar to the ones of the closest host tissue; interconnected pore structure with high porosity, allowing nutrients to penetrate the scaffold in vitro and vascularization to occur in vivo; suitable degradation rate, corresponding the speed of new bone generation; enough resistance to procedures and transportation before surgery; sterile environment for cell seeding [14], [15].

1.3.1. Biomaterials

There are three groups of biomaterials that one may use to fabricate scaffolds for bone tissue engineering applications: ceramics (e.g., hydroxyapatite, bioglass, biocements), natural polymers (e.g., chitosan, gelatin, collagen), and synthetic polymers (e.g., PCL, PEG, PLLA) [1], [16]. However, the brittle nature of ceramic materials and the difficulty controlling their degradation rate may limit their use in bone tissue engineering [1]. Also, synthetic polymers exhibit biocompatibility issues, release chemicals, and induce host reactions that cause clinical complications [17]. On the other hand, natural polymeric scaffolds provide great cell attachment, growth, and biocompatible and biodegradable properties [3]. ECM-based hydrogels are an example of this group of materials, and thus, they have been studied in tissue engineering [13].

1.3.1.1. ECM-based Hydrogels in Bone tissue engineering

ECM hydrogels are a promising group of materials in various fields (ophthalmology, burns/wounds healing, and drug delivery systems), including tissue engineering [18]. ECM-based hydrogels are based on natural polymeric materials, like gelatin, and collagen, possessing good biocompatibility properties with low cytotoxicity [19]. These materials are three-dimensional cross-linked hydrophilic polymeric chains that are biocompatible, flexible, soft, swell in an aqueous solution, and provide a suitable cell environment similar to the ECM [20]. Thus, enabling cell migration, adhesion, proliferation, and differentiation; and efficiently delivering nutrients and growth factors [20]. However, these biomaterials have poor mechanical properties and a fast degradation rate, limiting the range of applications and being necessary to change their structure and mechanics [18].

ECM hydrogels can be modified by altering the chemical (e.g., incorporating, in the polymeric chains, functional motives that can promote cell attachment), mechanical (e.g., alter the degree of cross-linking), and stimulus-responsive properties (e.g., load polymers with drugs or growth factors that can be released when stimulated) [21].

1.3.1.2. Collagen Type-I Hydrogels Scaffolds

Most collagen hydrogels are prepared using type I collagen since it is the main component of the extracellular matrix in the human body (approximately 90% of proteins in human connective tissues), and it is easily extracted from animal tissue without contamination by other collagens or NCPs [22]. Collagen provides structural integrity for tissues, high hydrophilicity, and high biodegradability with low inflammatory and cytotoxic responses [18], [19]. It has a significant impact on blood coagulation (promoting the aggregation of platelets) and mediating other ECM proteins' deposition [23]. Additionally, collagen can stimulate cell signalization processes involved in cell growth, proliferation, migration, and differentiation [18].

Collagen-based scaffolds may be fabricated either using collagen or using its denatured form (gelatin). However, to denature collagen into gelatin, acidic or alkaline solutions are used, and usually, the process is not complete. Thus the product obtained is generally a gelatinized collagen protein hydrogel [24]. When fabricating collagen hydrogel scaffolds, it is essential to choose the best processing conditions to obtain the desired properties. Some of the most important parameters to be considered are the solution's gelation time and temperature, and pH value. This way, one may find pH-sensitive and temperature-sensitive collagen hydrogels [24].

Several fabrication techniques have been used to fabricate collagen hydrogel scaffolds, including electrospinning [25], freeze-drying [26], sol-gel synthesis [27], and addictive manufacturing techniques [28].

1.3.2. Additive Manufacturing

Additive manufacturing (AM) principles have been applied for tissue engineering applications, including bone, cartilage, and skin regeneration [29]. 3D printing is the most known AM technique. It has tremendous capabilities, such as control internal architectures and porosity, precise deposition, cost-effectiveness, and tunable mechanical and structural properties [30].

3D printing of hydrogels through regular extrusion-based technologies is possible due to changing their composition by altering their concentration or adding additives that change their flow properties [31]. However, these materials present low-viscosity, and because of that, they tend to sag [28]. They must also be gelled *in situ* during the fabrication process and supported to not collapse or deform under their weight, making it difficult to print them with high fidelity beyond a few layers in height [32]. This way, 3D printing of biological hydrogels, like collagen, still needs significant improvement.

1.3.2.1. Suspension Printing

Suspension printing is a promising 3D printing technique based on extrusion bioprinting with a pressure-assisted microsyringe. Herein, low viscosity inks are extruded inside a suspension bath with a shear thinning behavior, so the created construct does not sag [32]. Shear-thinning behavior is typical of some non-Newtonian fluids. They exhibit solid-like characteristics in the absence of applied stress and fluid-like behavior when a stress greater than the fluid's yield stress is applied. This self-healing like capacity enables the suspension bath to behave like a liquid when the nozzle passes through a specific spot, allowing the ink to be extruded and behave as a solid once the needle leaves that particular site, as one can see in **Figure 3-a** [33]. This transition between liquid and solid enables the extruded filament to be trapped inside the bath. The suspension bath used in this kind of technique, besides the shear-thinning behavior, must support the soft structures being printed, promote cross-linking, and be removed after printing, as **Figure 3-b** shows [32].

In suspension 3D printing, it is essential to use suitable printing parameters: the distance between the nozzle and the bottom of the container where the bath is being held; the nozzle speed, which if it is too low, the filaments will be over-deposited, and if it is too high, the filaments will be stretched or even broken; the pressure controlling the flow rate at which the ink is being extruded, if it is too high, the filaments will be over-deposited, and if it is too low, no filaments will be printed.

This technique is being used in the last few years to print diverse biological structures, such as a model of a human femur, a model of a human right coronary arterial tree, a 3D brain model [32], a heart valve, and a model of a human heart [28].

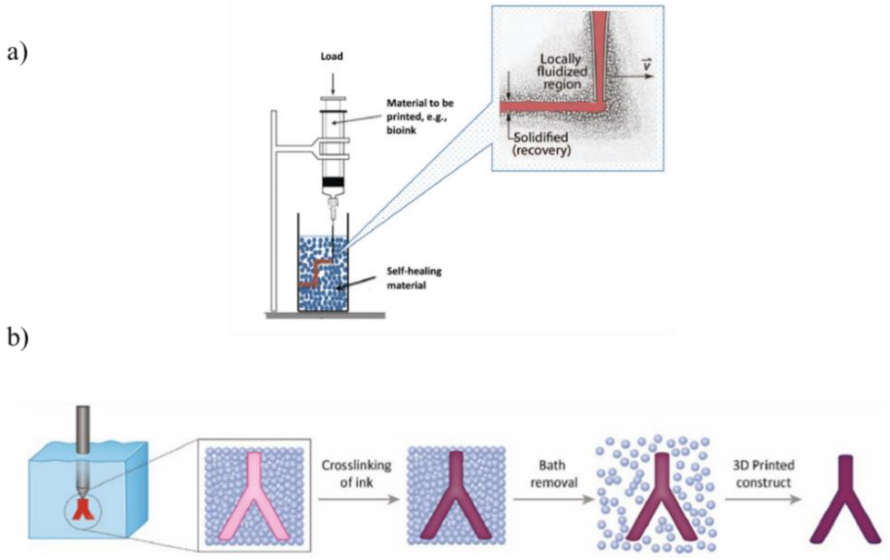

Figure 3*-Suspension 3D Printing Schematics and. a) Suspension printing set up with self-healing properties are shown. b) 3D construct removal from suspension bath. Retrieved from* [33].

1.3.2.2. Electrohydrodynamic Printing

Electrohydrodynamic printing (EHD) is an emerging AM technique that consists of a nozzle connected to a high voltage power supply and a grounded collector [34], creating an electric field between the nozzle and the collector. With the applied electric field, a Taylor cone is formed. Subsequently, a jet is stretched and accelerated towards the collector. This way, material flow is electrically driven, allowing fibers' fabrication with increased resolution compared to normal extrusion-based technologies [35][36]. However, EHD-printed scaffolds usually have a mean fiber diameter larger than several micrometers, which cannot mimic the sub-micro scale architectures in native ECM [35], making it imperative to introduce new approaches to increase the printing resolution.

In this thesis, we aim to print fibrillar collagen Type-I scaffolds using Suspension 3D printing to study the influence of collagen fibrils alignment in scaffolds mineralization under 10x PBS (mineralization solution), which has never been reported. Collagen cross-linking will take place through a rapid pH value change and temperature. We hypothesized that the thinner the printing filaments, the more aligned collagen fibrils would be, hence promoting either inter and intra-mineralization. We also introduced the suspended electrowriting technology, which has never been reported, using castor oil as the suspension bath, and assessing whether we could create a jet inside the oil.

2. Materials and Methods

2.1. Suspension bath Creation

The suspension bath was a gelatin slurry created using porcine gelatin type-A supplied from Sigma-Aldrich and 11 mM $CaCl_2$, following the same protocol described in [32].

2.2. Collagen ink Creation

A 10 mg/mL collagen ink was produced using slightly modified fibrillar bovine type-I collagen (**Figure 18**), purchased from Sigma-Aldrich and following the protocol described in **Appendix Section A**. Note that all the procedures were performed in an ice bath since collagen is temperature sensitive.

2.3. 3D Printing Setups

All our experiments were conducted using a custom grade 3D-printer (Stepcraft 420) modified to include a pressure valve connected to a syringe with a 25 G needle (**Figure 19**) and following the protocol described in **Appendix Section B**.

Figure 4 shows the two printing setups used: suspended printing and suspended electrowriting. Suspended printing (**Figure 4-a)**) was performed using a gelatin slurry as the suspension bath. Suspended electrowriting (**Figure 4-b)**) was conducted using self-made electrodes that could be fitted inside the Petri Dishes and commercial castor oil as a suspension bath. Two cables were used, one connected to the self-made electrode and the other connected to the nozzle. Both cables were also connected to a power supply.

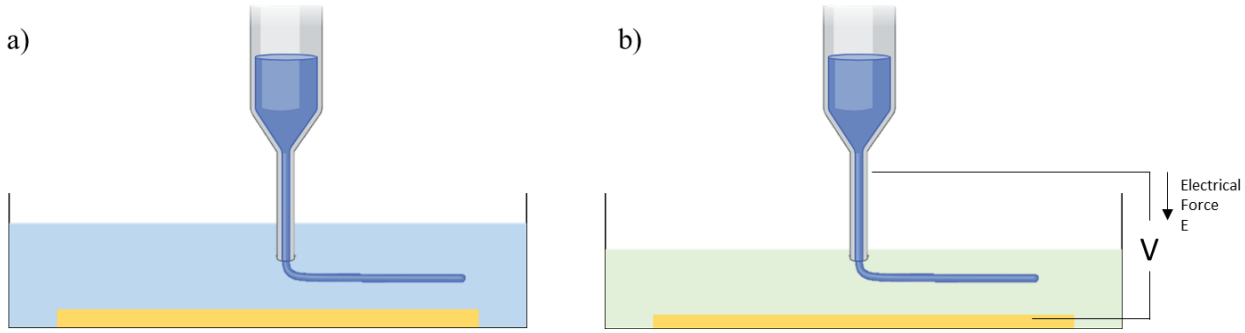

Figure 4*- a) Suspended Printing. b)Suspended Electrowriting Setup*

2.4. Characterization Techniques

2.4.1. Effect of key parameters on extruded printed filaments

To determine the minimum fiber diameter that we could obtain, samples with different printing speeds (5, 6, 7, 8, 9 mm/s) and flow rates (0.57, 0.64 µL/s) were imaged using an Olympus SZ61 stereoscope and measured with ImageJ.

2.4.2. Spreading Ratio

To determine the spreading ratio, square lattice constructs (1 cm x 1cm) were printed with ten layers and imaged using an Olympus SZ61 stereoscope. Fiber diameters were measured in 30 different locations using ImageJ software, and their values were compared with the needle inner diameter.

2.4.3. Swelling Ratio

To determine our collagen scaffolds' swelling, samples were imaged, and fibers were measured in the following time points: 0 days, 1 day, 4 days, and 7 days. Images were obtained using an Olympus SZ61 stereoscope, and fibers' diameters were measured using ImageJ software. The scaffolds were kept under 10x PBS, this one being replaced every day.

2.4.4. Collapsing Tests

Collapsing tests were conducted using self-made 3D molds and pillars, as shown in **Appendix Section C**. We printed straight filaments, without any suspension bath, inside castor oil, and a gelatin slurry. Each group's images were taken at three time points (t= 0s, t= 2 s, and t=4 s). A blue colorant was used to print inside the gelatin bath to facilitate the visibility of the filament.

2.4.5. Histology

Histology was performed on the collagen scaffolds using picrosirius red staining and polarized light microscopy to assess the collagen fibrils orientation after printing. Here the collagen scaffolds were first fixed under formalin for 24h. After fixed, samples were inserted in a tissue processor where they were embedded in paraffin. Next, samples were cut in a microtome and transferred to glass slides. Finally, samples were stained with picrosirius red, using the protocol in **Appendix Section D**, and imaged under polarized light in an Olympus BX 51 microscope.

2.4.6. Alizarin Red Staining

To assess our collagen's mineralization, samples were stained with alizarin red and imaged in the following time points: day 0, day 1, day 3, and day 7. Samples were fabricated for each time point analysis, giving a total of 8 samples. Here we washed our samples with demi-water at least 10 times before analysis. After being washed, the samples were stained with alizarin red for 5 min. Finally, the samples were rewashed (10 times) to wash out all the excess stain and imaged.

2.4.7. µCT

µCT was performed with an applied voltage of 90 kV, a field of view (FOV) of 30 µm, and a scan period of 3 min in a Quantum GX2 machine. Before starting the analysis, the samples were washed with demi-water several times to take out all the PBS from their surface.

2.4.8. Printing Accuracy

Theoretical models were created using a self-made Octave function and were compared to the experimental images obtained after printing. The displacement between theoretical and experimental constructs was measured.

2.5. Statistical Analysis

Data statistical analysis was performed using GraphPad Prism (San Diego, USA). The significant differences among the grouped data sets for printing optimization, swelling, spreading ratio, and suspended electrowriting were evaluated through Paired t-test. Type 1 error rate was set to 0.05, and the statistical significance was specified as *($p<0.05$), **($p<0.01$), ***($p<0.001$) and ****($p<0.0001$). ns means the groups' difference was not significant. A table with all the p values can be found in the **Appendix, section E**.

3. Results and Discussion

This dissertation's main goal was to study the influence of collagen fibrils alignment in collagen scaffolds mineralization. This way, collagen ink concentration was kept at 10 mg/mL, and collagen scaffolds were printed using a 25G needle and two flow rates: 0.57 and 0.64 µL/s. First, collagen scaffolds were printed with different nozzle speeds to assess the best printing condition, obtaining the minimum fiber diameter. Scaffolds were then printed using the best and worst resolutions and kept inside x10 PBS (mineralization solution). They were submitted to various characterization techniques, such as alizarin red staining, µCT, and histology. In this section, one can find all the results obtained and their respective discussion.

3.1. Extrusion printing of collagen in suspension baths

Before printing, we decided to test the suspension capability of two different materials (gelatin slurry and castor oil). To perform the tests, we had to build 3D molds, like the one presented in **Appendix Section C**. In this test, a single filament was printed on top of the orange pillars displayed in **Figure 5**.

Figure 5 shows that a filament can not be printed on top of the pillars without a suspension bath as it collapses instantly. In contrast, we were able to suspend a filament, as expected, when printing inside a gelatin slurry, considering Hinton *et al.* experiments using collagen and the same gelatin slurry bath [32]. Note that the ink extruded inside the gelatin bath was colored with a blue colorant to enhance the filament's visibility. The castor oil bath was also capable of supporting the extruded filament. However, we noticed the filament got sagged, meaning this bath does not present the rheological properties necessary for suspension 3D printing. We can also observe that 4 s after printing, the filaments are still suspended, meaning they maintain their integrity.

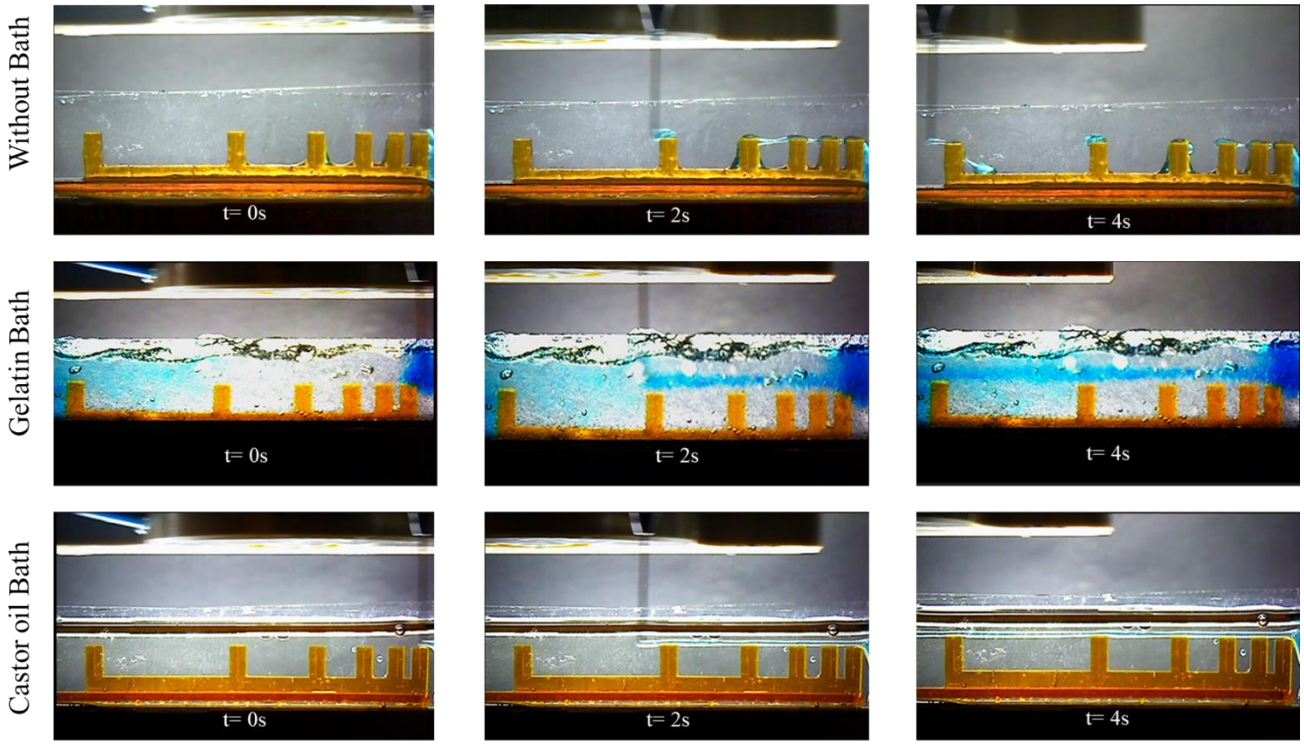

***Figure 5**- Collapsation tests performed without a suspension bath, inside a gelatin slurry bath, and inside castor oil.*

3.2. Effect of key parameters on extruded printed filaments

Hrynevich *et al.* 3D printed scaffolds using melt electrowriting technique, showing that the lower the flow rate and the faster the speed, the thinner the printed fiber will be, hence obtaining the best resolution. Conversely, the worst printing resolution would be obtained with a higher flow rate and a slower speed [29], as **Figure 6** shows. This way, we hypothesized that the same relationship would be valid for suspension printing.

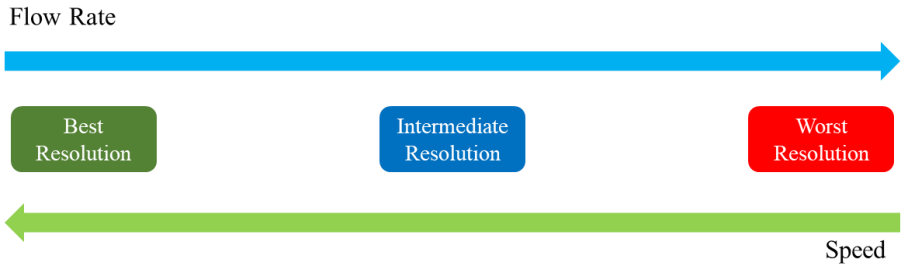

***Figure 6**-Schematic of the influence of flow rate and printing speed in printing resolution.*

With that in mind, printing optimization was performed using two flow rates (FR0.57 and FR0.64 µL/s) and five different velocities (5, 6, 7, 8, 9 mm/s). For FR0.57, we only tested two speeds (5 and 6 mm/s) since the filaments broke for higher values, the same happening for FR0.64 when values above 9 mm/s were used. **Figure 7** shows the effect of the printing parameters on fiber diameter, being clear that by maintaining the flow rate and increasing the speed, the fiber diameter decreases, which is in accordance with the results demonstrated in [29].

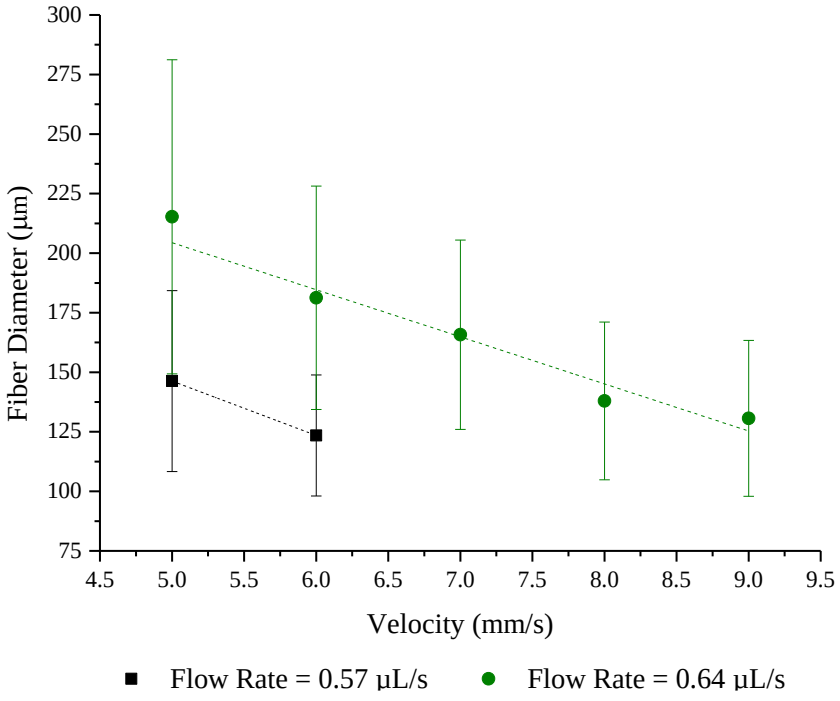

***Figure 7**- Effect of printing parameters (flow rate and velocity) in fiber diameter size.*

***Table 1**- Influence of Flow rate and speed on mean fiber diameter. Here, FR 0.57 corresponds to Flow rate = 0.57 µL/s and FR 0.64 corresponds to Flow rate = 0.64 µL/s.*

	Fiber Diameter (µm)				
Speed (mm/s)	**5**	**6**	**7**	**8**	**9**
FR 0.57	146 ± 38	123 ± 25	----	----	----
FR 0.64	215 ± 66	181 ± 47	166 ± 40	138 ± 33	131 ± 33

In **Figure 7** and **Table 1**, it is possible to notice that the smallest fiber diameter, with a mean diameter of 123 ± 25 µm, corresponds to the printing condition with a lower flow rate (FR0.57) and a speed of 6 mm/s. With a mean diameter of 215 ± 66 µm, the largest fiber diameter was obtained with a higher flow rate (FR0.64) and slower speed (5 mm/s), thus confirming our hypothesis. It is also relevant to point out that the smallest fiber diameter value corresponds to half the fibers' size obtained by Lee *et al.* when printing collagen inside a similar gelatin slurry bath [28].

One may also observe that the standard deviation bars are significant, which can be explained by the number of layers used to print the constructs. Here we used five layers to obtain the measured constructs, and in some positions, stackability might not be perfect, making it hard to distinguish single fibers.

From **Table 1,** one can observe a 23 µm difference between the fiber diameters obtained at 5 and 6 mm/s with a flowrate of FR0.57. Although this disparity seems minimal, it has a significance of * (p_v=0.0105). On the other hand, the difference between fiber diameters obtained at 6 mm/s with a flowrate of FR0.57 and 8 and 9 mm/s with an FR0.64 flow rate does not represent any statistical significance. Moreover, one can notice that the difference between the largest and the smallest fiber diameter is approximately 92 µm, with a significance of **** (p_v<0.0001). We believe that this difference strongly influences collagen fibrils alignment. This way, we chose the best and worst conditions to proceed with the characterization tests, comparing the collagen fibrils alignment and its influence on mineralization. The best and worst resolution printing conditions will be designated as **BR** and **WR**, respectively, and are represented in **Figure 8**.

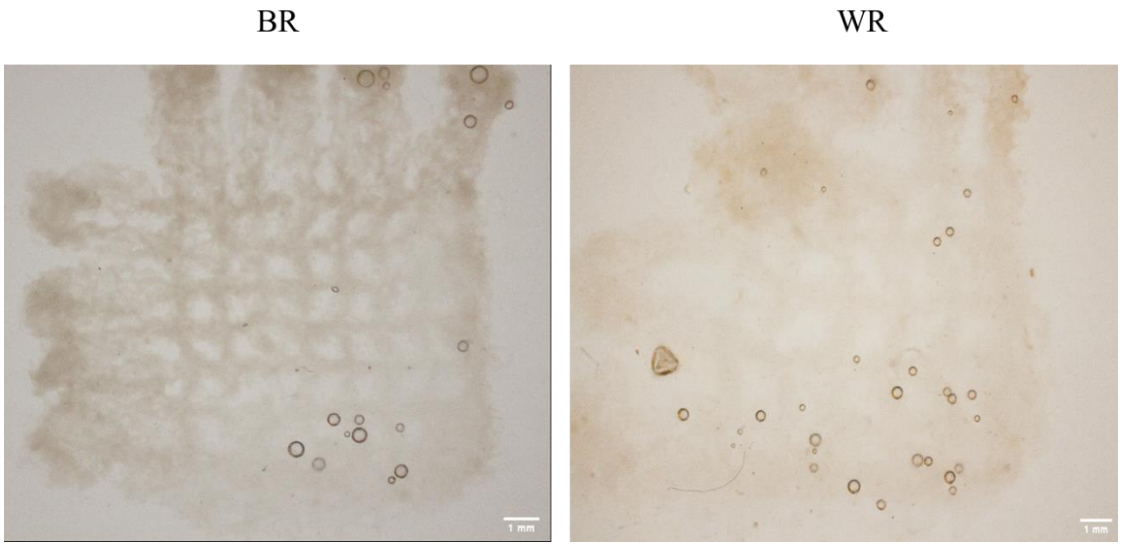

***Figure 8**- Best (BR) and Worst (WR) resolution of the printed scaffold*

3.3. Printing Accuracy of complex shaped designs

In the previous sections, we were able to print square scaffolds with an inner square lattice. However, we wanted to test more complex designs using the suspension printing technique. This way, we decided to print re-entrant auxetic scaffolds since auxetics are seen as a promising group for tissue engineering. Auxetics are materials, or structures, that exhibit a unique deformation behavior. Materials that behave conventionally expand (contract) axially while contracting (expanding) in the transverse direction. Meaning that these materials present a positive Poisson's ratio. On the other hand, auxetic materials, under tension (compression), tend to expand (contract) both axially and transversally due to their negative Poisson's ratio [37].

Here, we chose the best resolution printing condition (BR) to print the desired constructs. To test the Suspension printing technique's printing accuracy, we developed an Octave function in which we upload a threshold image from the printed scaffold and then compare it with the theoretical model. The function returns the displacement between the printed and theoretic points and an image with the experimental, theoretical, and comparison points, as shown in **Figure 9**.

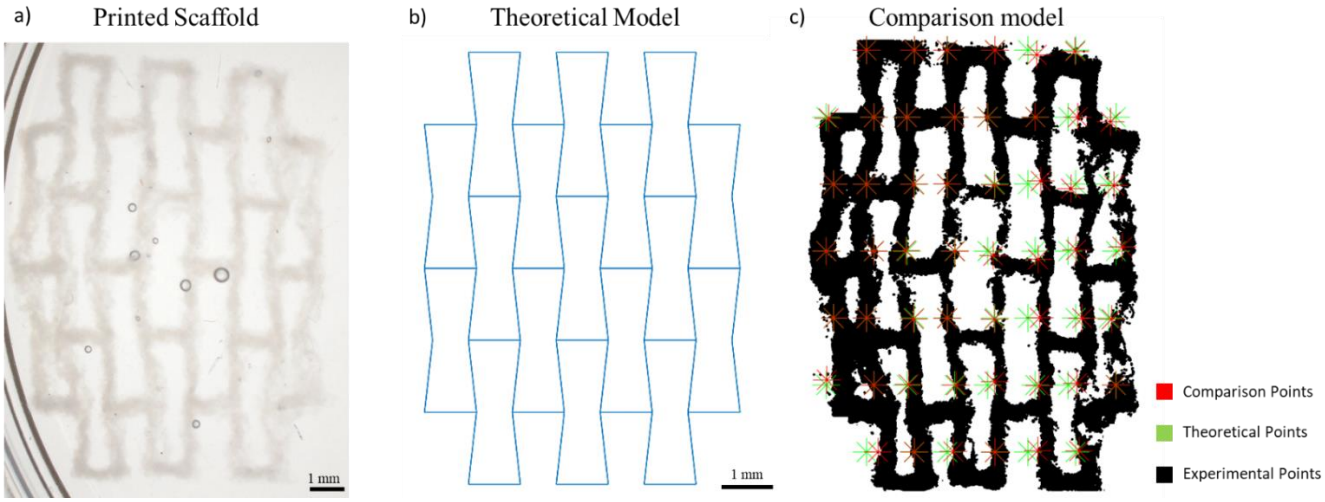

***Figure 9**- Comparison between the printed scaffold and the theoretical model designed using a self-made function in Octave. a) Printed Scaffold. b) Theoretical Model. c) Comparison Model.*

The displacement of the points from **Figure 9-c)** was 93 µm with a standard deviation (SD) of ± 107 µm, as shown in **Table 2**. The displacement value is not significantly high since we are printing scaffolds with several millimeters. However, the high SD value shows that the suspension 3D printing process of complex shaped designs still needs improvement.

***Table 2**-Mean displacement between the printed scaffold and the theoretical model*

Dist x (µm)	Dist y (µm)	Displacement (µm)
81 ± 102	31 ± 48	93 ± 107

3.3.1. Spreading Ratio

The spreading ratio (SPR) is defined as the ratio between the printed fiber diameter and the needle inner diameter [38], as indicated in **Equation 1**. An SPR value below 1.0 means the printed fiber was stretched during the printing process. Conversely, an SPR value above 1.0 indicates that the obtained fiber is swollen, while a value near 1.0 suggests an equivalent fiber diameter to the needle inner diameter, as shown in **Figure 10**.

$$SPR = \frac{Printed\ fiber\ diameter}{Needle\ inner\ diameter} \quad \textbf{Equation 1}$$

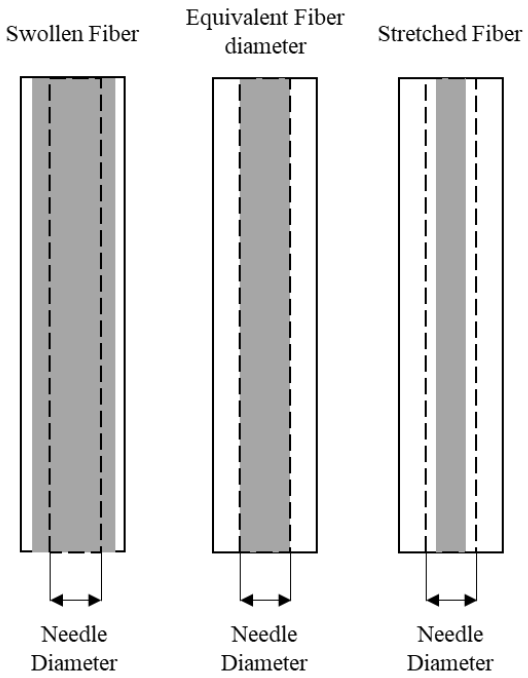

***Figure 10**-Relation between fiber diameter and needle inner diameter*

In this work, a 25G needle was used with an inner diameter of 0.26 mm. To quantify the SPR, fiber diameters from the scaffolds in **Figure 8** were measured in 30 different locations.

Table 3 presents the SPR for the BR and WR scaffolds printed, as we know, with different printing conditions. The worst resolution scaffold has an SPR of 0.83 with a standard deviation of 0.25. In contrast, the best resolution scaffold has an SPR of 0.47 with a standard deviation of 0.10. Both SPR values are below 1.0, meaning fibers were stretched during the printing process with a significant difference of **** (p_v<0.0001). These SPR values prove that WR scaffolds indeed have a worst resolution than the BR constructs, since lower SPR values are translated into higher precision scaffolds [38].

***Table 3**-Spreading Ratio of BR and WR scaffolds.*

	Spreading Ratio
BR	0.47 ± 0.10
WR	0.83 ± 0.25

3.4. Stability and fibril alignment of collagen scaffolds

3.4.1. Histology

Collagen fibers in native bone have a diameter of approximately 10 μm [39], compacting collagen fibrils inside them. The collagen fibril alignment is essential in scaffolds. Thus, without mimicking the alignment found in native tissues, it is impossible to build a biomimetic structure [40].

As it was said before, we printed fibrillar collagen scaffolds. This way, we hypothesized that the shear and extensional flows during printing and consequent compaction would promote the fibrils alignment; hence, the best resolution (BR) scaffolds, having a mean fiber diameter of 123 μm, would present more aligned collagen fibrils than the worst resolution (WR) scaffold with a mean fiber diameter of 215 μm. This theory is supported by Nerger *et al.'s* work, where it was shown that collagen alignment increased with a fiber diameter size reduction [41].

Samples with the best and worst resolution were compared with a control group consisting of human trabecular bone. The samples were stained with picrosirius red staining and imaged using polarized light microscopy. Picrosirius red bonds to collagen molecules, making it possible to distinguish collagen segments from other components present in our samples under polarized light microscopy.

In **Figure 11**, one can recognize three groups: control group, BR, and WR. In the control group, we can observe well-defined and arranged collagen fibers, which is in line with the analysis performed by F. Rauch *et al.* to bone under polarized light microscopy [42]. In this group, one may notice structures with considerable light intensity, which can be explained by the high collagen concentration present in the bone sample. In the BR and WR group, the light intensity is not very high, meaning there is a low concentration of collagen molecules in the samples. There is no preferential alignment of the WR group's collagen fibrils, being arranged in various directions. There are also several yellow streaks that are not collagen, but defects from the histology process. In contrast, in the BR group, we can observe the collagen fibrils' preferential alignment despite the low collagen concentration. In fact, in the **40x** magnification, we can see well-defined and aligned fibrils, similar to those found in the control group. This fibril preferential alignment is in line with Nerger et al.'s research [41]. However, collagen alignment in scaffolds fabricated via suspension printing has never been reported.

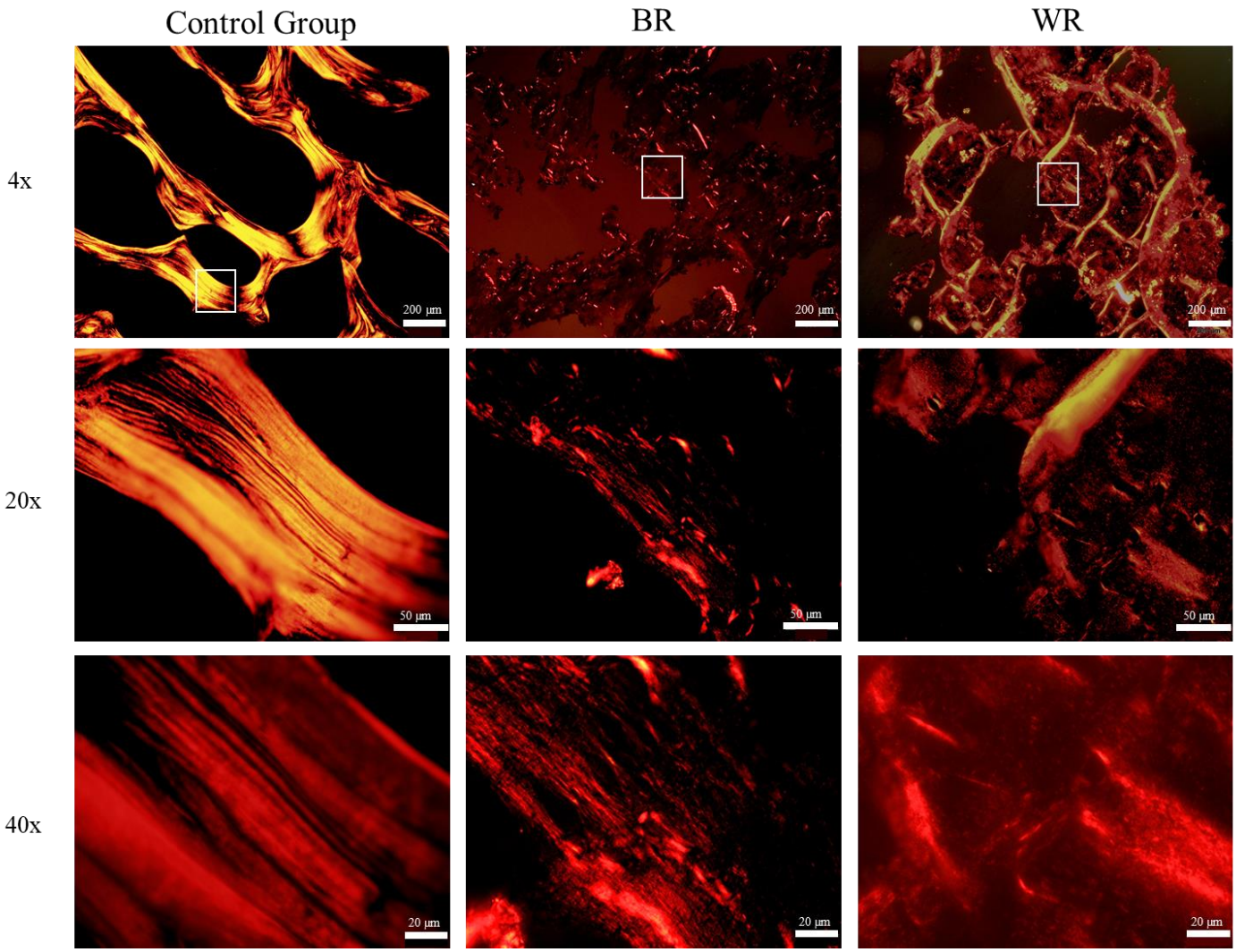

***Figure 11**- Polarized light microscope images with 4x, 20x, and 40x magnification. Control Group – Sample from a portion of bovine bone. BR – Best resolution sample with aligned collagen fibers. WR – Worst resolution, with no alignment found.*

3.4.2. Swelling Ratio

Swelling ratio is an important parameter once it suggests the scaffolds' behavior when in contact with blood and other body fluids [43]. This way, scaffold's swelling was observed in four time points after printing (day 0, day 1, day 4, and day 7) in the BR and WR scaffolds, and fiber diameters were measured in ten different locations in each scaffold. One can notice, in **Figure 12-a)** and **Table 4**, that the mean fiber diameter of both scaffolds increases with the passing of days. On day 0, the BR and WR scaffolds' mean fiber diameter is 269 ± 37 and 317 ± 32 µm, respectively, with a significant difference of * (p_v=0.0177). After 7 days, the mean fiber diameter of the BR and WR scaffolds increased to 381 ± 33 µm and 438 ± 29 µm, respectively, translating in an approximately 120 µm disparity between days 0 and 7. The values on day 0 are higher than those presented in the printing optimization section for the best and worst scaffold's resolution. This difference is explained by the number of layers used to print the constructs and poor fiber's stackability. In this part of the work, samples with ten layers were printed.

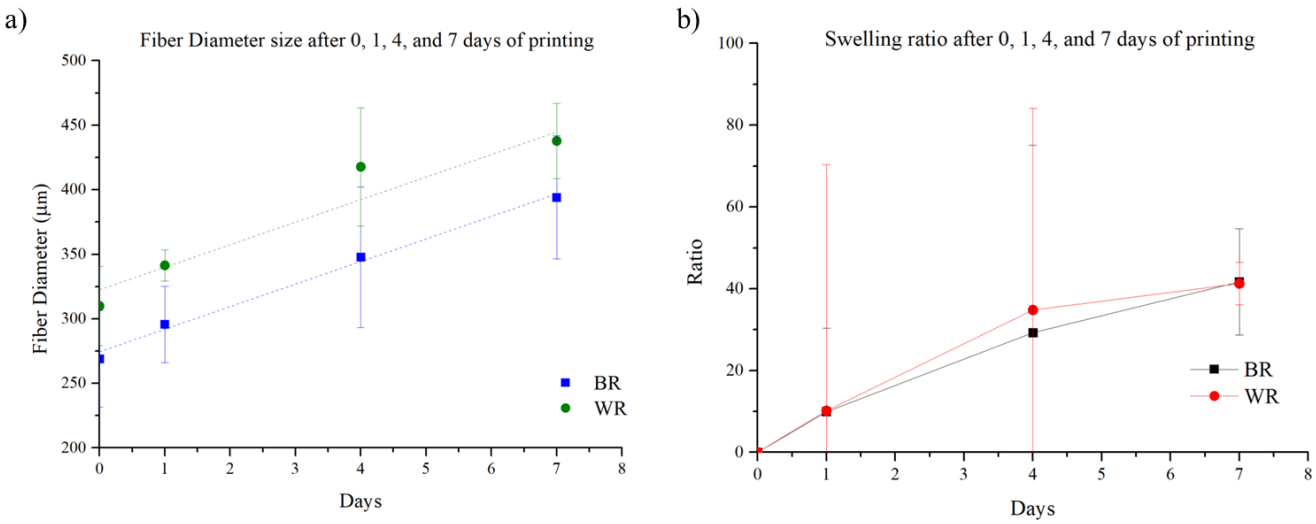

***Figure 12**-a) Fiber diameter size and b) Swelling ratio after, 0,1,4, and 7 days of printing.*

By looking at **Figure 12-b)** and **Table 4**, we can see that both samples' swelling ratios appear to be quite similar with no significant (ns) differences (p_v=0.4378) since both samples show approximately 42% swelling after 7 days. However, it was expected, the WR's swelling ratio to be smaller than BR's, as filaments are closer to each other, resulting in limited expansion. Moreover, we can conclude that even after 7 days under x10 PBS, scaffolds maintain most of their integrity.

However, these results do not follow the swelling ratios of collagen scaffolds presented in the literature. For instance, Nocera, *et al.* 3D printed fibrillar collagen hydrogel scaffolds with a swelling ratio of 1437 % ± 146 % [44]. This discrepancy might be explained by the osmotic pressure between the scaffolds and the mineralization solution, which has a high salt concentration. Hence, both the scaffold and the surrounding solution are saturated. Consequently, the amount of water entering the scaffold is minimal, thus explaining the low swelling ratio value.

***Table 4**-Fiber diameter values and swelling ratio after 0, 1, 4, and 7 days of printing*

	Fiber diameter (µm)		**Swelling Ratio (%)**	
Days after printing	**BR**	**WR**	**BR**	**WR**
0	269 ± 37	310 ± 31	0	0
1	296 ± 30	341 ± 12	10 ± 21	10 ± 60
4	348 ± 55	418 ± 46	29 ± 46	35 ± 49
7	381 ± 33	438 ± 29	42 ± 13	41 ± 5

3.5. *In Vitro* Mineralization

We believe that collagen fibrils alignment may promote mineral deposition in the inter and intrafibrillar spaces, thus promoting scaffolds' mineralization. Note that scaffolds were printed inside a gelatin slurry with calcium chloride ($CaCl_2$). For mineralization to occur, scaffolds were maintained in a mineralization solution (x10 PBS) after printing. 10x PBS was chosen as the mineralization solution since it has disodium phosphate (Na_2HPO_4) in its content, and so, phosphate ions, one of the predominant ions in the bone's mineral phase. When in contact, PBS and $CaCl_2$ react and may form dicalcium phosphate ($CaHPO_4$) and sodium chloride (NaCl), as it is shown below. This way, the reaction product is a CaP that, as said in the introduction section, is one of the most abundant mineral phases in bone tissue [3].

$$CaCl_2 + Na_2HPO_4 \leftrightarrow NaCl + CaHPO_4$$

3.5.1. Alizarin Red Staining

Alizarin Red Staining (ARS) is commonly used to identify calcium in tissue sections, and it is a destructive technique since the staining process is unreversible, meaning the sample can not be reused. Calcium forms a complex with ARS, and the product is a bright red stain. For this part of the work, we fabricated samples for each time point analysis.

Figure 13 shows stained scaffolds imaged in three time points after printing (day 0, day 1, day 3). On **day 0,** one can notice the presence of calcium ions in both scaffolds, as they were printed inside a $CaCl_2$ media. Nevertheless, we can observe a low color intensity on this day, meaning fewer calcium ions in the scaffolds.

One day after printing (**day 1**), we can verify that the bright red stain's intensity in the BR scaffold increases, indicating that more calcium ions were deposited. However, color intensity remained constant in the WR sample. In contrast, on **day 3**, we can observe an increase in the bright red stain's color intensity in both groups. One can also see that the red stain in the BR sample is more abundant than in the WR scaffold, meaning a discrepancy in the amount of calcium present in both samples. The amount of minerals present in the WR scaffold on day 3 also suggests that mineral deposition increased between **days 1** and **3**.

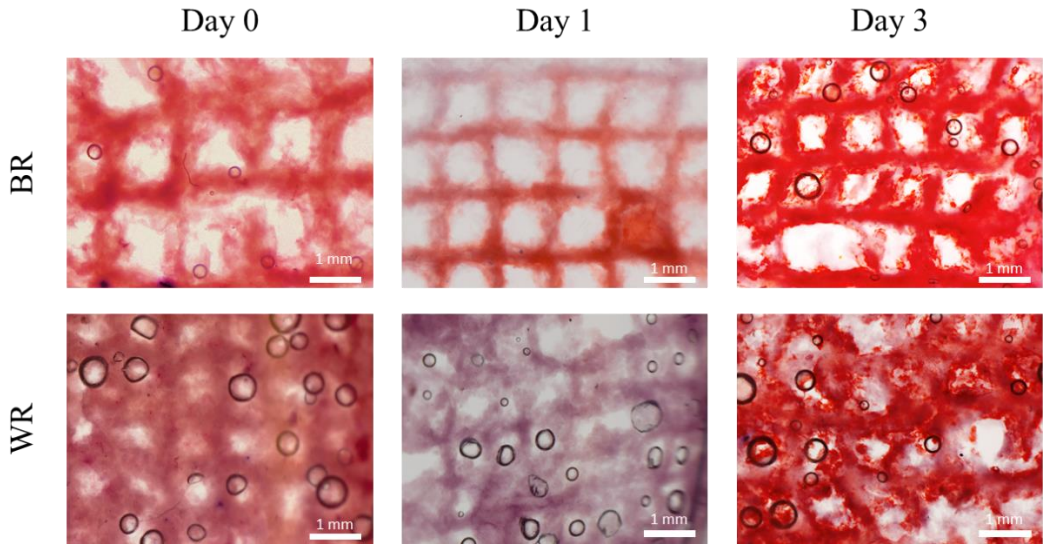

***Figure 13**-Stereoscope Alizarin Red Staining images taken in four time points after printing (day 0, day 1, and day 3) using x2 magnification.*

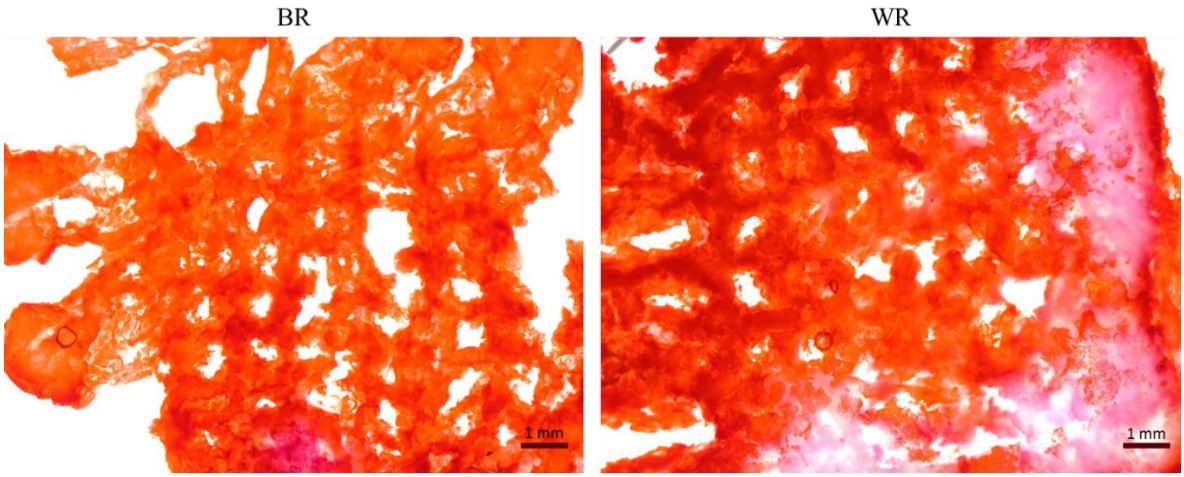

***Figure 14**- Stereoscope Alizarin Red Staining image taken after 7 days of printing, using x1 magnification.*

In **Figure 14**, we can see pictures taken 7 days after printing. We can observe a significant difference between the BR and WR groups. Here one can see that, after 7 days, the bright red stain covers the whole scaffold in the BR group, suggesting the scaffold is entirely covered with calcium. However, the WR scaffold shows large white spots, which means that is still space available for mineral precipitation.

These results show that collagen fiber alignment might have a significant influence on scaffold's mineralization. However, more tests should be conducted so our results can be proved. Moreover, we can neither infer the locations (intra and interfibrillar spaces) where minerals were deposited nor the mechanism by which mineralization occurs. Nevertheless, we believe that intra and interfibrillar mineral deposition occurs in the BR scaffold, as fibrils are more compacted and aligned. In contrast, the WR scaffold is expected to mostly present intrafibrillar mineralization since it is predominant [6].

3.5.2. µCT

Despite the obtained results with alizarin red staining, we wanted to assess the scaffolds' mineral disposition. To evaluate it, we decided to perform a µCT analysis on both samples (BR and WR). The analysis was performed after the samples were submerged for 14 days under x10 PBS (mineralization solution). Before the analysis, the samples were washed several times to take all the non-attached minerals out, and liquid media was taken out of the Petri dish.

Figure 15-A and **B** show the printed scaffolds imaged on the stereoscope, and **Figure 15-C** and **D** presents the scaffolds imaged through µCT. By analyzing the micro-CT's images, one can notice two different significant colors, white and grey. The grey color represents unmineralized spots, while the white color corresponds to minerals.

Figure 15- C and **D** show well-defined scaffolds similar to those represented in **Figure 15-A** and **B**. Regardless of the similarity, one can not identify the scaffolds' pores, which can be explained by the lack of liquid media during the µCT analysis. Once the liquid was taken out, the construct's surface adopted a spherical shape, closing the scaffold's pores. Concerning the mineral disposition along the scaffolds, we can observe a considerable area occupied mostly with white spots, meaning both scaffolds are in an advanced mineralization state after 14 days submerged under x10 PBS. These results are in tune with the results obtained in the alizarin red staining section and Gao. C *et al.*'s results, where a collagen scaffold showed high levels of mineralization after 15 days [45].

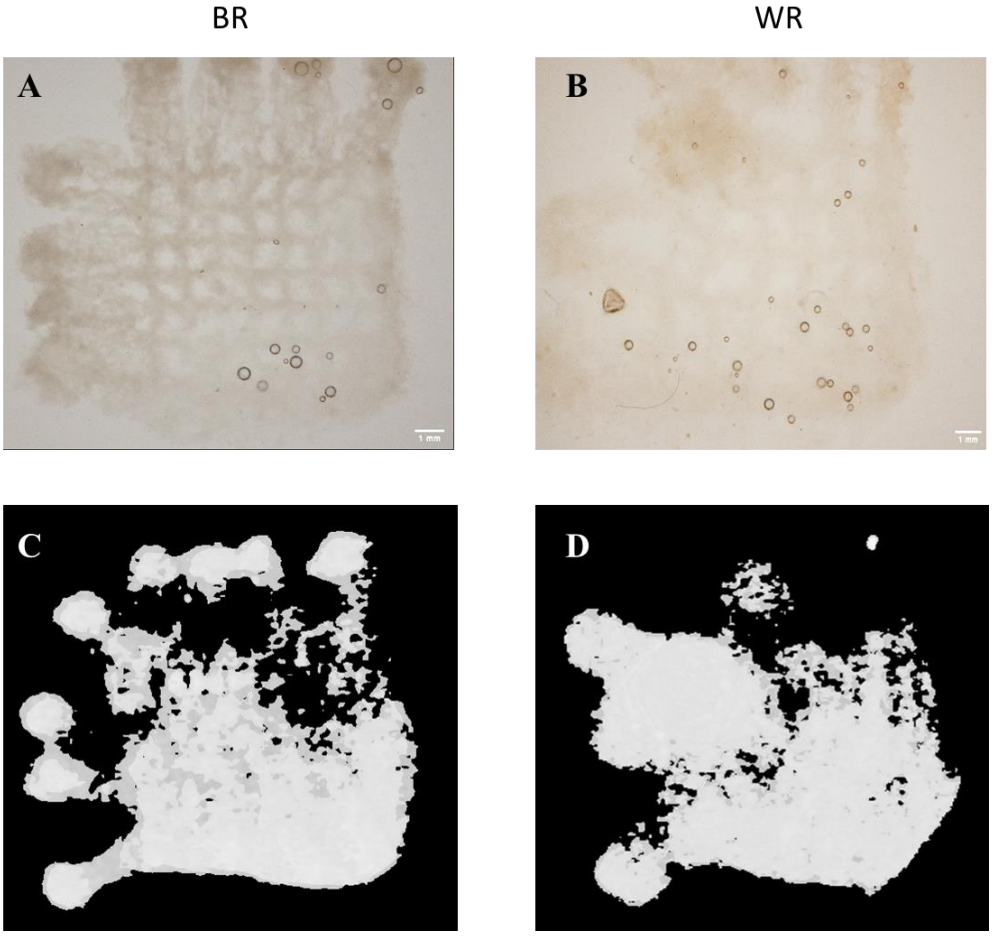

Figure 15*-Printed Scaffolds and µCT analysis. A- BR scaffold. B- WR scaffold. C- BR scaffold imaged through µCT analysis. D- WR scaffold imaged through µCT analysis. All images were taken after 14 days under x10 PBS (mineralization solution). Grey and white color represent unmineralized and mineralized spots, respectively.*

3.6. Effect of electrical field on fiber diameter

To increase resolution, reach smaller fiber diameters, and, consequently, promote fibril alignment, we introduce a new technique, called suspended electrowriting (SEW).

Suspended Electrowriting is a technology based on Suspension Printing and Electrohydrodynamic (EHD) printing principles, and it has never been reported. This technology is seen as a promising technique for printing hydrogels with a high resolution, combining suspension baths with an electric field, as seen in **Figure 4-b)**.

The main challenge of suspended electrowriting is finding a suspension bath that combines both desired rheological and electrical properties. The bath needs to support the printed filament (shear-thinning behavior) and behave like an electric isolator. Despite not having the appropriate rheological properties, we chose the vegetable oil family, specifically castor oil, to proceed with our investigation. Castor oil is highly viscous (η=1.023 ± 0.02 Pa.s) compared to other vegetable oils, non-conductive with a dielectric constant of ε=4.5 [46], cheap, and can be bought in a regular cosmetic store.

Figure 16 shows a mathematical model that predicts the jet behavior when extruded inside the oil bath or in the air with and without the electric field's influence. As we can observe in both media, the jet decreases its diameter once the electric field is applied. This phenomenon is explained by the Taylor cone formation and subsequent stretching of the electrically driven jet, which are the basic principles of the electrowriting process [47]. With this model creation, we can prove theoretically that with suspended electrowriting, we can achieve better resolutions when it comes down to hydrogels' 3D print inside oil baths.

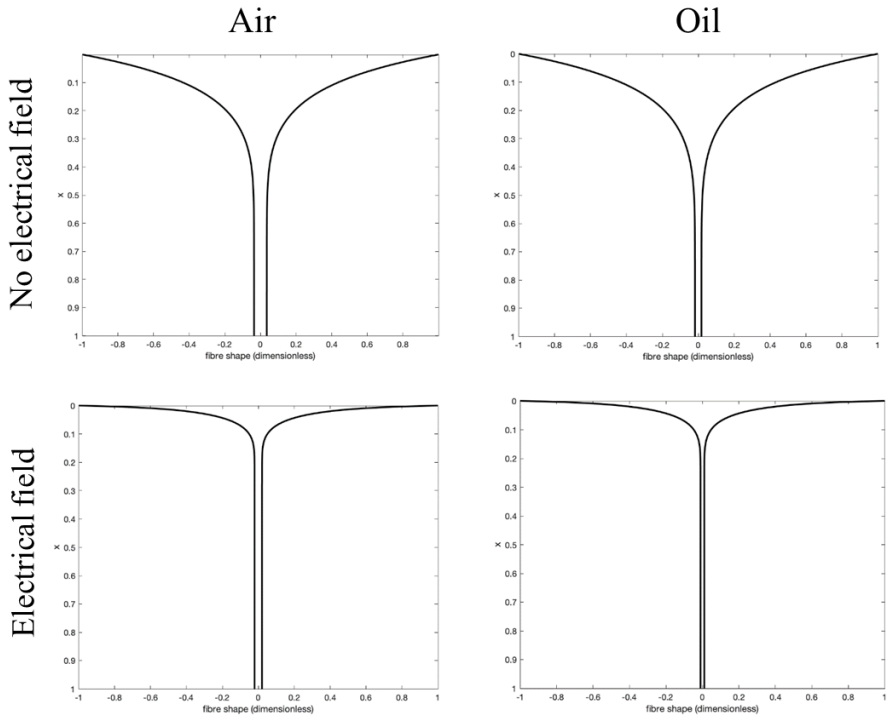

***Figure 16**- Theoretical models, predicting jet diameter inside air and oil with and without an applied electric field. Model developed by Dr. Miguel Castilho (Assistant Professor at UMC Utrecht).*

Figure 17 shows the jet formation with and without an electric field in air and inside castor oil. One can notice that the jet is extruding a large volume of material both in air and castor oil, with jet diameters of 466 and 720 µm (**Table 5**), respectively, without the presence of an electric

field and the same flow rate. These jet diameters values are not in accordance with the theoretical model since the jet in castor oil is 250 µm bigger than the jet formed in the air with a significance of **** (p_v<0.0001). The high hydrophobicity of castor oil, and the collagen-ink's high-water content may explain this jet diameter difference. Water tends to adopt a spherical shape inside a continuous oil media since that conformation provides the minimum surface tension. As we can see in **Figure 17-a)**, the collagen-ink forms round edges both in air and in oil. However, in castor oil, the spherical shape is more evident.

In contrast, one may observe, in **Figure 17-b)**, that with an applied electric field, jets formed both in air and inside castor oil decrease their diameter size. One may also notice that the jet formed inside the oil is smaller than the jet formed in air when an electric field is applied, with jet diameters of 40 and 152 µm (**Table 5**), respectively, following the theoretical prediction. This disparity between both diameters has a significance of *** (p_v=0.0004), and it can be explained by the Taylor cone formation. Inside castor oil, we can see the Taylor cone creation and the subsequent jet acceleration. Note that the Taylor cone is of extreme importance as it enables the jet to be stretched and, consequently, reduces its diameter.

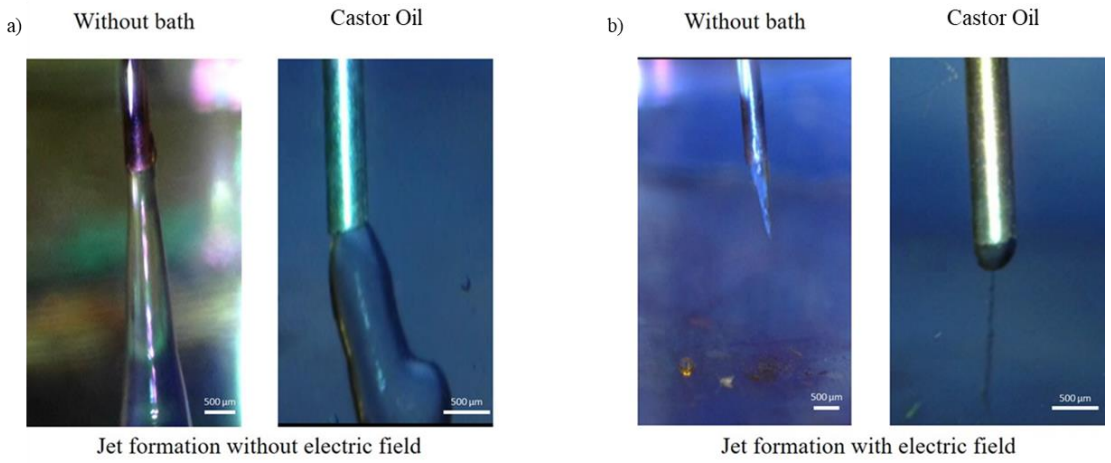

***Figure 17**-Jet formation inside castor oil and without suspension bath. a) Jet formed without an applied electric field. b) Jet formed with the presence of an electric field.*

***Table 5**-Jet diameter variation with and without bath and electric field*

Ø 0,5 mm Needle	**Without Bath**	**Castor Oil**
E=0	466 ± 18	720 ± 20
E>0	152 ± 7	40 ± 5

Although we could form a well-defined jet inside castor oil, we could print neither a filament nor a construct since the filaments sagged. Despite castor oil's viscosity, it lacks the shear-thinning behavior, which is essential for the filaments to be trapped inside the bath. Moreover, we noticed that the jet acceleration forces (electric field and gravity) were significantly higher than the oil's yield stress. So, collagen was always being deposited on top of the bottom electrode, thus creating a short-circuit. This way, more investigation concerning the suspension baths for suspended electrowritting needs to be performed.

4. Conclusion and Future Perspectives

This project was developed in the Orthopaedics Department of University Medical Centre Utrecht (UMC). The main goal was to study the influence of collagen fibrils alignment in collagen scaffolds mineralization. Therefore, fibrillar collagen scaffolds were printed using suspension 3D printing with different fiber resolutions since we hypothesized that fiber diameter influences fibril alignment.

First, extrusion printing of collagen in suspension baths was conducted to assess the suspension capability of castor oil and gelatin slurry. The filaments were suspended on both baths without collapsing, indicating that constructs do not need extra support to be printed. However, it was noticed that during printing inside castor oil, that the filament sagged, meaning the castor oil bath lacks the needed shear-thinning behavior, and suspension is only achieved due to the viscous behavior of the oil bath.

After proving the gelatin slurry's suspension capability, we optimized the printing parameters by changing the flow rate at which the ink was extruded and the nozzle speed. A mean fiber diameter of 123 ± 25 µm was achieved, with a spreading ratio of 0.47 ± 0.10 for the best printing condition (BR), while a fiber diameter of 215 ± 66 µm with a spreading ratio of 0.83 ± 0.25 for the worst printing condition (WR). The spreading ratio of both scaffolds indicates that printed fibers were indeed stretched during the printing process. One way of reducing the fiber stretching during printing is to use needles with smaller inner diameters.

Accuracy of the printing method when printing complex shaped designs was also evaluated. For this purpose, we printed re-entrant auxetic constructs and compared them with a theoretical 3D model developed on Octave. The displacement between both models (theoretic and experimental) was 93 ± 107 µm, which is not significantly different when working at the macroscale. However, this result suggests the printing process needs improvements and that the printing resolution must be increased, allowing us to work with precision at the nano or microscale to better mimic the native bone ECM.

Concerning the evaluation of stability and fiber alignment, histology with picrosirius red staining was performed under polarized light microscopy. Here, we were able to observe a preferential alignment in the BR samples and an unorganized fiber arrangement in the WR scaffold. These observations proved that the fiber diameter size influences the collagen fiber alignment. The scaffold's swelling ratio was also calculated, obtaining a 42% ratio and concluding that the constructs remain stable after 7 days submerged in 10x PBS.

For the mineralization tests, alizarin red staining of BR and WR scaffolds was done in four time points after printing: day 0, day 1, day 4, and day 7. BR scaffolds started to show mineral precipitation signs one day after being submerged in the mineralization solution. In contrast, the WR scaffolds only showed mineral deposition signs after three submersion days in 10x PBS. As a complementary test to ARS, µ-CT was performed to prove scaffolds mineralization and to show the mineral disposition along the scaffold. Scaffolds were analyzed after 14 days in the mineralization solution, both showing to be in an advanced state of mineralization, with minerals deposited along the constructs. These results seem to show that collagen fiber alignment has a significant influence on scaffold's mineralization. However, more studies should be conducted to increase the statistical support and conclude if collagen alignment does really affects mineral precipitation. Moreover, we could not infer the locations (intra and interfibrillar spaces) where minerals were deposited.

Despite the results obtained, scaffold's resolution must be increased to mimic the native ECM's microstructure. To increase the printing resolution, hence promoting more collagen fibril alignment and, consequently, mineralization, we started studying a never-reported printing technology called suspended electrowriting (SEW). We were able to create an electrically driven jet inside a castor oil bath with a diameter of 40 µm, which is considerably different from the jet diameter of 720 µm obtained in castor oil without an applied electric field.

Future investigation in this matter should be focused on TEM analysis to assess where minerals were deposited inside the collagen scaffold and help to fully understand the impact of fibril alignment in the mineralization mechanism; Mechanical tests since the goal is to create suitable bone grafts; And seeding cells into the scaffolds to assess cell attachment and proliferation. Moreover, SEW technology must be thoroughly investigated to increase the scaffolds' resolution and, as a result, better mimic the native bone microstructure. This technique's main challenge is to find a material with proper rheological and electrical properties to print electrically driven filaments. This way, oleogels seem to be a valid group of materials to be used as suspension baths for suspended electrowriting, as they are mainly composed of oils and have the rheological properties suitable for this kind of printing.

5. References

[1] E. J. Sheehy, D. J. Kelly, and F. J. O'Brien, "Biomaterial-based endochondral bone regeneration: a shift from traditional tissue engineering paradigms to developmentally inspired strategies," *Mater. Today Bio*, vol. 3, p. 100009, 2019, doi: 10.1016/j.mtbio.2019.100009.

[2] J. Y. Rho, L. Kuhn-Spearing, and P. Zioupos, "Mechanical properties and the hierarchical structure of bone," *Med. Eng. Phys.*, vol. 20, no. 2, pp. 92–102, 1998, doi: 10.1016/S1350-4533(98)00007-1.

[3] P. Chocholata, V. Kulda, and V. Babuska, "Fabrication of scaffolds for bone-tissue regeneration," *Materials (Basel).*, vol. 12, no. 4, p. 568, 2019, doi: 10.3390/ma12040568.

[4] E. Hamed, Y. Lee, and I. Jasiuk, "Multiscale modeling of elastic properties of cortical bone," *Acta Mech.*, vol. 213, pp. 131–154, 2010, doi: 10.1007/s00707-010-0326-5.

[5] X. Lin, S. Patil, Y. G. Gao, and A. Qian, "The Bone Extracellular Matrix in Bone Formation and Regeneration," *Front. Pharmacol.*, vol. 11, pp. 1–15, 2020, doi: 10.3389/fphar.2020.00757.

[6] M. Murshed, "Mechanism of Bone Mineralization," *Cold Spring Harb. Perspect. Med.*, vol. 8, pp. 1–12, 2018, doi: 10.1101/cshperspect.a031229.

[7] F. Nudelman, A. J. Lausch, N. A. J. M. Sommerdijk, and E. D. Sone, "In vitro models of collagen biomineralization," *J. Struct. Biol.*, vol. 183, no. 2, pp. 258–269, 2013, doi: 10.1016/j.jsb.2013.04.003.

[8] W. J. Landis and M. J. Song, "Early mineral deposition in calcifying tendon characterized by high voltage electron microscopy and three-dimensional graphic imaging," *J. Struct. Biol.*, vol. 107, no. 2, pp. 116–127, 1991, doi: https://doi.org/10.1016/1047-8477(91)90015-O.

[9] A. S. Deshpande and E. Beniash, "Bioinspired Synthesis of Mineralized Collagen Fibrils," *Cryst. Growth Des.*, vol. 8, no. 8, pp. 3084–3090, 2008, doi: 10.1021/cg800252f.

[10] R. Dimitriou, E. Jones, D. McGonagle, and P. V. Giannoudis, "Bone regeneration: Current concepts and future directions," *BMC Med.*, vol. 9, p. 66, 2011, doi: 10.1186/1741-7015-9-66.

[11] C. Dhand *et al.*, "Bio-inspired in situ crosslinking and mineralization of electrospun collagen scaffolds for bone tissue engineering," *Biomaterials*, vol. 104, pp. 323–338, 2016, doi: 10.1016/j.biomaterials.2016.07.007.

[12] V. Raeisdasteh Hokmabad, S. Davaran, A. Ramazani, and R. Salehi, "Design and fabrication of porous biodegradable scaffolds: a strategy for tissue engineering," *J. Biomater. Sci. Polym. Ed.*, vol. 28, no. 16, pp. 1797–1825, 2017, doi: 10.1080/09205063.2017.1354674.

[13] G. S. Hussey, J. L. Dziki, and S. F. Badylak, "Extracellular matrix-based materials for regenerative medicine," *Nat. Rev. Mater.*, vol. 3, no. 7, pp. 159–173, 2018, doi: 10.1038/s41578-018-0023-x.

[14] S. Bose, M. Roy, and A. Bandyopadhyay, "Recent advances in bone tissue engineering scaffolds," *Trends Biotechnol.*, vol. 30, no. 10, pp. 546–554, 2012, doi: 10.1016/j.tibtech.2012.07.005.

[15] G. M. Cunniffe, G. R. Dickson, S. Partap, K. T. Stanton, and F. J. O'Brien, "Development and characterisation of a collagen nano-hydroxyapatite composite scaffold for bone tissue engineering.," *J. Mater. Sci. Mater. Med.*, vol. 21, no. 8, pp. 2293–2298, 2010, doi: 10.1007/s10856-009-3964-1.

[16] S. Afewerki, A. Sheikhi, S. Kannan, S. Ahadian, and A. Khademhosseini, “Gelatin-polysaccharide composite scaffolds for 3D cell culture and tissue engineering: Towards natural therapeutics,” *Bioeng. Transl. Med.*, vol. 4, no. 1, pp. 96–115, 2019, doi: 10.1002/btm2.10124.

[17] D. A. Wahl and J. T. Czernuszka, “Collagen-hydroxyapatite composites for hard tissue repair,” *Eur. Cells Mater.*, vol. 11, pp. 43–56, 2006, doi: 10.22203/eCM.v011a06.

[18] J. A. Claudio-Rizo, J. Delgado, I. A. Quintero-Ortega, J. L. Mata-Mata, and B. Mendoza-Novelo, “Decellularized ECM-Derived Hydrogels: Modification and Properties,” *Hydrogels*, pp. 3–22, 2018, doi: 10.5772/intechopen.78331.

[19] S. Dinescu, M. Albu Kaya, L. Chitoiu, S. Ignat, D. A. Kaya, and M. Costache, “Collagen-Based Hydrogels and Their Applications for Tissue Engineering and Regenerative Medicine,” in *Cellulose-Based Superabsorbent Hydrogels*, M. I. H. Mondal, Ed. Cham: Springer International Publishing, 2018, pp. 1–21.

[20] M. Liu *et al.*, “Injectable hydrogels for cartilage and bone tissue engineering,” *Bone Res.*, vol. 5, 2017, doi: 10.1038/boneres.2017.14.

[21] S. Utech and A. R. Boccaccini, “A review of hydrogel-based composites for biomedical applications: enhancement of hydrogel properties by addition of rigid inorganic fillers,” *J. Mater. Sci.*, vol. 51, no. 1, pp. 271–310, 2016, doi: 10.1007/s10853-015-9382-5.

[22] E. E. Antoine, P. P. Vlachos, and M. N. Rylander, “Review of collagen I hydrogels for bioengineered tissue microenvironments: characterization of mechanics, structure, and transport.,” *Tissue Eng. Part B. Rev.*, vol. 20, no. 6, pp. 683–696, 2014, doi: 10.1089/ten.TEB.2014.0086.

[23] K. Gelse, E. Pöschl, and T. Aigner, “Collagens--structure, function, and biosynthesis.,” *Adv. Drug Deliv. Rev.*, vol. 55, no. 12, pp. 1531–1546, 2003, doi: 10.1016/j.addr.2003.08.002.

[24] V. Perez-Puyana, M. Jiménez-Rosado, A. Romero, and A. Guerrero, “Fabrication and Characterization of Hydrogels Based on Gelatinised Collagen with Potential Application in Tissue Engineering,” *Polymers (Basel).*, vol. 12, no. 5, 2020, doi: 10.3390/polym12051146.

[25] Y. Wakuda, S. Nishimoto, S. Suye, and S. Fujita, “Native collagen hydrogel nanofibres with anisotropic structure using core-shell electrospinning,” *Sci. Rep.*, vol. 8, no. 1, p. 6248, 2018, doi: 10.1038/s41598-018-24700-9.

[26] C. J. Lowe, I. M. Reucroft, M. C. Grota, and D. I. Shreiber, “Production of Highly Aligned Collagen Scaffolds by Freeze-drying of Self-assembled, Fibrillar Collagen Gels.,” *ACS Biomater. Sci. Eng.*, vol. 2, no. 4, pp. 643–651, 2016, doi: 10.1021/acsbiomaterials.6b00036.

[27] C. Echalier *et al.*, “Sol–gel synthesis of collagen-inspired peptide hydrogel,” *Mater. Today*, vol. 20, no. 2, pp. 59–66, 2017, doi: https://doi.org/10.1016/j.mattod.2017.02.001.

[28] A. Lee *et al.*, “3D bioprinting of collagen to rebuild components of the human heart,” *Science (80-.).*, vol. 365, no. 6452, pp. 482–487, 2019, doi: 10.1126/science.aav9051.

[29] A. Hrynevich *et al.*, “Dimension-Based Design of Melt Electrowritten Scaffolds,” *Small*, vol. 14, no. 22, pp. 1–6, 2018, doi: 10.1002/smll.201800232.

[30] C. F. Marques, G. S. Diogo, S. Pina, J. M. Oliveira, T. H. Silva, and R. L. Reis, “Collagen-based bioinks for hard tissue engineering applications: a comprehensive review,” *J. Mater. Sci. Mater. Med.*, vol. 30, no. 3, p. 32, 2019, doi: 10.1007/s10856-019-6234-x.

[31] N. Ashammakhi *et al.*, “Advancing Frontiers in Bone Bioprinting.,” *Adv. Healthc. Mater.*, vol. 8, no. 7, p. e1801048, Apr. 2019, doi: 10.1002/adhm.201801048.

[32] T. J. Hinton *et al.*, “Three-dimensional printing of complex biological structures by freeform reversible embedding of suspended hydrogels,” *Sci. Adv.*, vol. 1, no. 9, 2015, doi: 10.1126/sciadv.1500758.

[33] A. McCormack, C. B. Highley, N. R. Leslie, and F. P. W. Melchels, “3D Printing in Suspension Baths: Keeping the Promises of Bioprinting Afloat,” *Trends Biotechnol.*, vol. 38, no. 6, pp. 584–593, 2020, doi: 10.1016/j.tibtech.2019.12.020.

[34] Y. Wu, B. Wu, S. Vijayavenkataraman, Y. S. Wong, and J. Y. H. Fuh, “Crimped fiber with controllable patterns fabricated via electrohydrodynamic jet printing,” *Mater. Des.*, vol. 131, pp. 384–393, 2017, doi: https://doi.org/10.1016/j.matdes.2017.06.027.

[35] B. Zhang, J. He, Q. Lei, and D. Li, “Electrohydrodynamic printing of sub-microscale fibrous architectures with improved cell adhesion capacity,” *Virtual Phys. Prototyp.*, vol. 15, no. 1, pp. 62–74, 2020, doi: 10.1080/17452759.2019.1662991.

[36] M. Castilho *et al.*, “Hydrogel-Based Bioinks for Cell Electrowriting of Well-Organized Living Structures with Micrometer-Scale Resolution,” *Biomacromolecules*, 2021, doi: 10.1021/acs.biomac.0c01577.

[37] P. Mardling, A. Alderson, N. Jordan-Mahy, and C. L. Le Maitre, “The use of auxetic materials in tissue engineering,” *Biomater. Sci.*, vol. 8, no. 8, pp. 2074–2083, 2020, doi: 10.1039/c9bm01928f.

[38] F. E. Freeman and D. J. Kelly, “Tuning Alginate Bioink Stiffness and Composition for Controlled Growth Factor Delivery and to Spatially Direct MSC Fate within Bioprinted Tissues,” *Sci. Rep.*, vol. 7, no. 1, p. 17042, 2017, doi: 10.1038/s41598-017-17286-1.

[39] M. J. Buehler, “Nature designs tough collagen: Explaining the nanostructure of collagen fibrils,” *Proc. Natl. Acad. Sci.*, vol. 103, no. 33, pp. 12285 LP – 12290, 2006, doi: 10.1073/pnas.0603216103.

[40] U. Cheema, “2 - Three-dimensional collagen biomatrix development and control,” in *Standardisation in Cell and Tissue Engineering*, V. B. T.-S. in C. and T. E. Salih, Ed. Woodhead Publishing, 2013, pp. 18–33.

[41] B. A. Nerger, P.-T. Brun, and C. M. Nelson, “Microextrusion printing cell-laden networks of type I collagen with patterned fiber alignment and geometry,” *Soft Matter*, vol. 15, no. 28, pp. 5728–5738, 2019, doi: 10.1039/C8SM02605J.

[42] F. Rauch, R. Travers, A. M. Parfitt, and F. H. Glorieux, “Static and dynamic bone histomorphometry in children with osteogenesis imperfecta.,” *Bone*, vol. 26, no. 6, pp. 581–589, 2000, doi: 10.1016/s8756-3282(00)00269-6.

[43] S. A. Ghodbane and M. G. Dunn, “Physical and mechanical properties of cross-linked type I collagen scaffolds derived from bovine, porcine, and ovine tendons,” *J. Biomed. Mater. Res. A*, vol. 104, no. 11, pp. 2685–2692, 2016, doi: 10.1002/jbm.a.35813.

[44] A. D. Nocera, R. Comín, N. A. Salvatierra, and M. P. Cid, “Development of 3D printed fibrillar collagen scaffold for tissue engineering,” *Biomed. Microdevices*, vol. 20, no. 2, p. 26, 2018, doi: 10.1007/s10544-018-0270-z.

[45] C. Gao *et al.*, “MSC-seeded dense collagen scaffolds with a bolus dose of VEGF promote healing of large bone defects,” *Eur. Cell. Mater.*, vol. 26, pp. 195–207, 2013, doi: 10.22203/eCM.v026a14.

[46] S. Calligaris, L. Manzocco, S. Pieve, G. Arrighetti, and M. Nicoli, “Effect of Lipid Physical State of Palm Derivatives on β-Carotene Bleaching,” *J. Food Sci.*, vol. 78, 2013, doi: 10.1111/1750-3841.12087.

[47] B. Zaarour, L. Zhu, and X. Jin, “A Review on the Secondary Surface Morphology of Electrospun Nanofibers: Formation Mechanisms, Characterizations, and Applications,” *ChemistrySelect*, vol. 5, no. 4, pp. 1335–1348, 2020, doi: 10.1002/slct.201903981.

Appendix

A. Collagen ink Creation

First, collagen was transferred to 50 mL falcon tubes, freeze-dried for 24 h, and then blended for 30 s in an IKA's blender (A11 basic Analytical mill, Ref: 0002900000). After blending, 400 mg of collagen were weighed and dissolved in 40 mL of 0.3% (v/v) acetic acid, with constant low stirring speed (150 rpm) and temperature (T = 4 ºC), for at least 24h. This way, a solution of 10 mg/mL concentration was created. After the dissolving process, the solution was blended for 120 s and transferred to 50 mL falcon tubes. To remove all bubbles, the solution was centrifuged for 5 min at 3000 rpm, and T=4 ºC. Finally, the collagen-ink can be stored at 4 ºC. All these procedures were performed in an ice bath since collagen is temperature-sensitive.

***Figure 18**-Schematic with the various levels of collagen organization.*

B. 3D Printing Setup

The gelatin slurry and the collagen-ink were transferred to the 3.5 cm diameter Petri dishes and the syringe, respectively, using a gel pipette, reducing bubbles both in the bath and the ink. Next, a needle of 0.5 mm outer diameter (25 G) was used to perform all the experiments. After printing, the Petri dishes were covered with a lid and put on a heating plate set to 35 ºC for at least 2 hours to promote collagen temperature-dependent cross-linking and gelatin slurry melting. After cross-linking is complete, the gelatin is taken out of the Petri dishes and replaced by 10x PBS (mineralization solution).

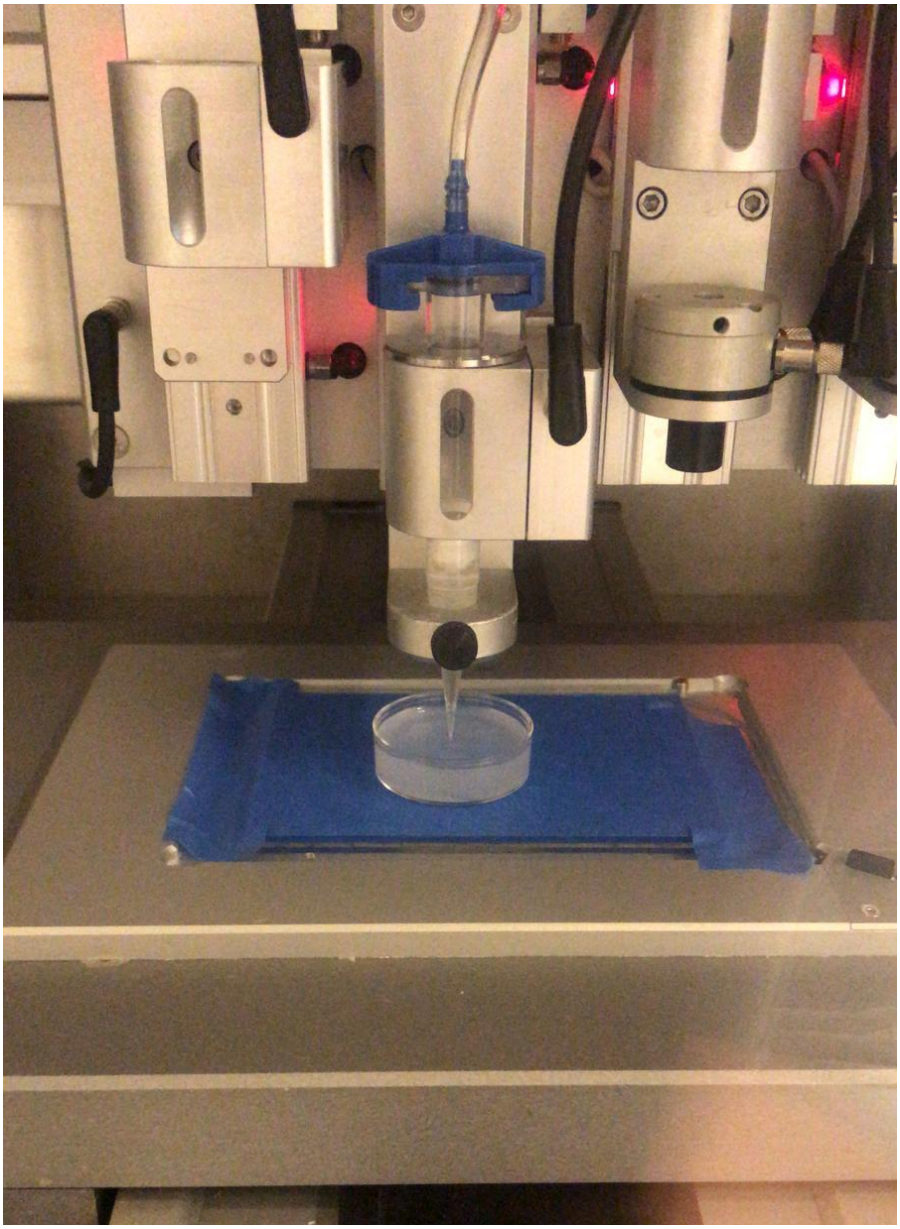

Figure 19*- Setup similar to the one used in this work.*

C. Collapsation Tests

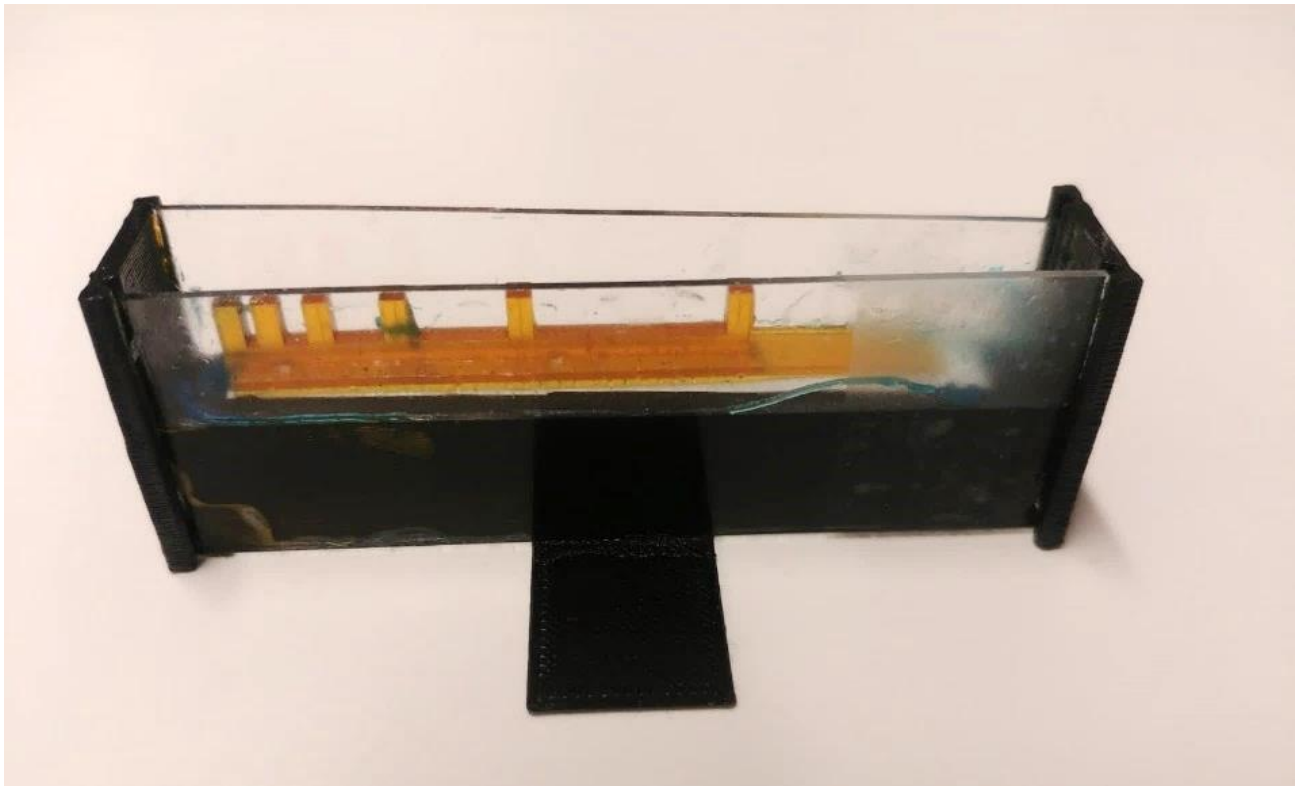

***Figure 20**- 3D printed molds with pillarlets to use in collapsing tests.*

D. Picrosirius Red Staining Protocol

The picrosirius red stain was created by mixing 0.1 g Sirius red F3B (Klinipath No.80115) with 100 mL saturated aqueous picric acid (Riedel-deHaën No.36011).

After the stain was prepared, we were able to start the staining protocol. First, we deparaffined the cut sections with nine solutions (Xylene 100%, 90%, 70%, 70%, Ethanol 100%, 90%, 70%, 70%, and demi-water), by rinsing the samples for 2 min with each solution. After the deparaffinization process, samples were stained with picrosirius red for 1 h. Next, to fix the stain on the samples, they were rinsed in 0.01M HCl for 2 min. The stained samples must then be dehydrated using eight solutions (Ethanol 100%, 90%, 70%, 70%, and Xylene 100%, 90%, 70%, 70%) and mount in depex. Finally, samples were dried for at least 12h inside a fume hood.

E. Statistical Analysis

***Table 6**-Statistical analysis for printing optimization, swelling ratio, and suspended electrowriting.*

Technique	Compositions	p-value	Summary	Significant
Printing Optimization	5 mm/s_FR0.57 vs 6mm/s_FR0.57	0.0105	*	Yes
	5mm/s_FR0.57 vs 5mm/s_FR0.64	<0.0001	****	Yes
	5mm/s_FR0.57 vs 6mm/s_FR0.64	0.0081	**	Yes
	5mm/s_FR0.57 vs 7mm/s_FR0.64	0.0369	*	Yes
	5mm/s_FR0.57 vs 8mm/s_FR0.64	0.2495	ns	No
	5mm/s_FR0.57 vs 9mm/s_FR0.64	0.0728	ns	No
	6mm/s_FR0.57 vs 5mm/s_FR0.64	<0.0001	****	Yes
	6mm/s_FR0.57 vs 6mm/s_FR0.64	<0.0001	****	Yes
	6mm/s_FR0.57 vs 7mm/s_FR0.64	<0.0001	****	Yes
	6mm/s_FR0.57 vs 8mm/s_FR0.64	0.0403	*	Yes
	6mm/s_FR0.57 vs 9mm/s_FR0.64	0.3351	ns	No
	5mm/s_FR0.64 vs 6mm/s_FR0.64	0.0082	**	Yes
	5mm/s_FR0.64 vs 7mm/s_FR0.64	0.0002	***	Yes
	5mm/s_FR0.64 vs 8mm/s_FR0.64	<0.0001	****	Yes
	5mm/s_FR0.64 vs 9mm/s_FR0.64	<0.0001	****	Yes
	6mm/s_FR0.64 vs 7mm/s_FR0.64	0.1652	ns	No
	6mm/s_FR0.64 vs 8mm/s_FR0.64	0.0014	**	Yes
	6mm/s_FR0.64 vs 9mm/s_FR0.64	<0.0001	****	Yes
	7mm/s_FR0.64 vs 8mm/s_FR0.64	0.0021	**	Yes
	7mm/s_FR0.64 vs 9mm/s_FR0.64	0.0021	**	Yes
	8mm/s_FR0.64 vs 9mm/s_FR0.64	0.3514	ns	No

Spreading Ratio	BR vs WR	<0.0001	****	Yes
Swelling Ratio	BR vs WR (Day 0) - Fiber diameter	0.0177	*	Yes
	BR vs WR (Day 1) - Fiber diameter	0.0021	**	Yes
	BR vs WR (Day 4) - Fiber diameter	0.0032	**	Yes
	BR vs WR (Day 7) - Fiber diameter	0.004	**	Yes
	BR vs WR - Ratio	0.4378	ns	No
Suspended Electrowriting	Air vs Castor Oil	<0.0001	****	Yes
	Air vs Castor Oil with E>0	<0.0001	****	Yes
	Air vs Air with E>0	<0.0001	****	Yes
	Air with E>0 vs Castor Oil with E>0	0.0004	***	Yes
	Air E>0-Castor Oil	<0.0001	****	Yes
	Castor Oil vs Castor Oil with E>0	<0.0001	****	Yes